J. Fluid Mech. (2014), *vol.* 742, *pp* 520–551.
doi:10.1017/jfm.2013.686

Streak evolution in viscoelastic Couette flow

Jacob Page and Tamer A. Zaki†

Department of Mechanical Engineering, Imperial College, London SW7 2AZ, UK

(Received 3 June 2013; revised 3 November 2013; accepted 19 December 2013)

The combined effect of inertia and elasticity on streak amplification in planar Couette flow of an Oldroyd-B fluid is examined. The linear perturbation equations are solved in the form of a forced-response problem to obtain the wall-normal vorticity response to a decaying streamwise vortex. With significant disparity between the solvent diffusion and polymer relaxation time scales, two distinct responses are possible. The first is termed 'quasi-Newtonian' because the streak evolution collapses onto the Newtonian behaviour at the same total and solvent Reynolds numbers when relaxation is very fast or slow, respectively. The second response is labelled 'elastic': with a long relaxation time, the streaks can reach significant amplitudes even with very weak inertia. If the diffusion and relaxation time scales are commensurate, the streaks are able to re-energize in a periodic cycle within an envelope of overall decay. This behaviour is enhanced in the instantaneously elastic limit, where the governing equation reduces to a forced wave equation. The streak re-energization is demonstrated to be a superposition of trapped vorticity waves.

Key words: transition to turbulence, viscoelasticity

1. Introduction

The fluid dynamics of viscoelastic liquids often defies intuition gleaned from the study of Newtonian flows. A good example is the linear instability in zero-Reynolds-number flows with streamline curvature (Shaqfeh 1996). This phenomenon vanishes in the limit of zero curvature, but recent work has shown the potential for significant transient amplification of disturbances in parallel, inertialess flows (Jovanovic & Kumar 2010). Interestingly, the most amplifying events are streak-like perturbations in the streamwise velocity, the same flow structures observed in high-Reynolds-number Newtonian flows. In this work, the transient streak amplification in response to forcing by a decaying streamwise vortex is investigated using the linear perturbation equations. The evolution of the streaks displays a rich variety of dynamical behaviours, which depend on the ratio of the solvent diffusion time scale and the relaxation time of the polymer. The analysis offers a new perspective on the phenomenon of transient growth in highly elastic, weakly inertial flows, and also identifies a new regime where the transmission of information via wave propagation leads to streaks which re-energize many times before eventual decay.

† Present address: Department of Mechanical Engineering, Johns Hopkins University, Baltimore, MD 21218, USA. Email address for correspondence: t.zaki@imperial.ac.uk

1.1. *Transient growth in viscoelastic fluids*

Non-modal stability analyses have shown that short-time energy amplification can be achieved in flows which are linearly stable. This result is possible owing to the fact that the eigenvectors of the stability operator are non-orthogonal (Butler & Farrell 1992; Schmid & Henningson 2001). Physically, this energy growth is associated with well-understood mechanisms. Short-time growth is predominantly driven by the wall-normal displacement of mean momentum, referred to as lift-up (Landahl 1980). Perturbations with vanishing streamwise dependence are typically found to be most amplifying, and so the transient behaviour of the optimal disturbance describes the growth and decay of streamwise-aligned streaky structures. This is consistent with experimental observations of the early stages of transition in noisy environments. One example is the agreement of the optimal disturbance analysis (Andersson, Berggren & Henningson 1999) with experimental measurements of the streamwise velocity perturbations in transitional boundary layers beneath free-stream turbulence. In reality, the streaks can reach a sufficiently large amplitude to be subject to secondary instabilities from which breakdown to turbulence follows (Vaughan & Zaki 2011).

Recently, an analogy has been proposed between transient growth in high-Reynolds-number Newtonian flows and strongly elastic flows of polymer solutions (Jovanovic & Kumar 2010, 2011; Lieu, Jovanović & Kumar 2013). This rests on a similarity between the lift-up term in the momentum equation and polymer stretching terms in the constitutive relation. The polymer stretching mechanism was first identified through consideration of a class of pure stress perturbations to Couette flow of an Oldroyd-B fluid. These stress perturbations are divergence free, and hence do not contribute any forcing in the momentum equations (Kupferman 2005; Doering, Eckhardt & Schumacher 2006; Renardy 2009). In the polymer conformation equation, they undergo transient amplification due to polymer stretching by the base-flow shear, and they ultimately decay due to relaxation. Since the polymer evolution equations for an Oldroyd-B fluid are linear in the stress, the divergence-free stress perturbations remain admissible solutions in the linearized and fully nonlinear flow problems. As such, they alone cannot be the initial seed for transition to turbulence since they do not couple to the nonlinear terms in the momentum equations (Renardy 2009).

The ability of viscoelastic fluids to support short-time kinetic energy growth has been established by Hoda, Jovanović & Kumar (2008, 2009). They investigated the response of channel flow of an Oldroyd-B fluid to stochastic body forcing, which is introduced as an input to the momentum equations. Therefore, the polymer plays a subservient role in the ensuing dynamics. It was found that increasing the relative contribution of the polymer to the total viscosity significantly enhanced the energy density of the response. Also of interest is the fact that the response showed peaks at non-zero frequencies, in contrast to the Newtonian problem. The new time scales introduced with the polymer dynamics were cited as being responsible for this shift (Hoda *et al.* 2009). More recently, Zhang *et al.* (2013) computed optimal velocity disturbances in channel flow of a FENE-P fluid with large inertia, at sub-critical Reynolds number. Elasticity was found to enhance the amplification of streamwise streaks relative to the Newtonian flow.

Jovanovic & Kumar (2010) established that significant kinetic energy amplification can be achieved in the absence of inertia altogether. Their work explored the effects of initial conditions in the polymer stresses on transient growth of the streamwise velocity. Non-zero initial stress perturbations are essential since the velocity field is enslaved to the dynamics of the polymers. Accordingly, the growth mechanism was shown to be polymer stretching by background shear, the same mechanism responsible for the transient amplification of pure stress perturbations. The polymer stretching results in the emergence of a body force in the streamwise momentum equation, leading to streaks in the streamwise velocity. The initial polymer stresses responsible for streak formation are those in the cross-flow plane. Since the rate of decay is now set by the relaxation time, the potential for energy amplification scales as W^2, where W is the Weissenberg number. This corresponds to an $O(W)$ streak amplitude. Further work by Jovanovic & Kumar (2011) used singular perturbation methods to investigate energy amplification due to stochastic body forces in the weak-inertia, high-elasticity limit. Their analysis provides further evidence of similarities between polymer stretching in highly elastic flows and tilting of mean vorticity in high-Reynolds-number Newtonian flows. Recently, these results have been extended to a more realistic polymer model, where the large energy growth generated by polymer stretch is upper bounded by the maximum extensibility of the polymer chains (Lieu *et al.* 2013).

Significant energy amplification in elastic flows with inertia can form a pathway to bypass transition to a disordered state termed 'elasto-inertial turbulence' (Dubief, Terrapon & Soria 2013; Samanta *et al.* 2013). This phenomenon has been found experimentally to be sustained at lower Reynolds numbers than Newtonian turbulence. However, it is distinct from 'elastic turbulence', a term coined to describe the chaotic state seen experimentally at negligible Reynolds numbers (Groisman & Steinberg 2000; Larson 2000). Elastic turbulence is triggered by the linear elastic instability in flows with streamline curvature. More recently, Pan *et al.* (2013) reported based on experimental evidence that elastic turbulence can be realized in parallel flows using finite-amplitude perturbations.

1.2. *Hyperbolicity in instantaneously elastic fluids*

In a Newtonian fluid, the transient response to a decaying streamwise vortex is the short-time growth of a spanwise row of high- and low-speed streaks. The streaks are dominated by their streamwise velocity perturbation, u, which initially amplifies and subsequently decays due to viscosity (Butler & Farrell 1992; Reddy & Henningson 1993; Schmid 2007). It is curious to consider how the introduction of viscoelastic effects augments this process. For instance, in Poiseuille flow of shear-thinning fluids, a reduction in the viscosity close to the wall has a stabilizing effect and reduces the propensity for energy amplification due to the altered shear distribution (Nouar, Bottaro & Brancher 2007). However, in fluids exhibiting stress memory and relaxation, the introduction of hyperbolic polymer dynamics means that a simple modification of the Newtonian solution is not likely. Instead, entirely new patterns of behaviour can be anticipated.

The growth of streamwise-oriented streaks in an Oldroyd-B fluid is shown here to be governed by a wave equation with damping. A similar operator has appeared in the viscoelastic literature before, but in a different context: it governs the evolution of the velocity field in one-dimensional, time-dependent shear flows (Joseph 1990). For example, Tanner (1962) solved the viscoelastic equivalent of Stokes' first problem. For very dilute polymer solutions, the behaviour resembles a Newtonian fluid, whereby information propagates upwards through the diffusion of vorticity. However, if the solvent contribution to the viscosity vanishes, the governing equation becomes hyperbolic. Consequently, the vorticity discontinuity propagates upwards as a shear wave, with a speed fixed by the properties of the fluid. The wave is damped by the relaxation of the polymer. Without a solvent viscosity, the shock is not smoothed.

This solution has formed the theoretical underpinning for a device that measures the shear wave speed for elastic liquids (Joseph, Narain & Riccius 1986). A thorough overview of solutions to variations on this problem is given by Preziosi & Joseph (1987).

Of significant relevance to transient streak growth in viscoelastic liquids is the analogous problem of impulsively started Couette flow. As described above, the discontinuity in the vorticity propagates away from the moving wall as a shear wave in the instantaneously elastic limit, a behaviour which diminishes as the solvent contribution to the total viscosity is increased. Denn & Porteous (1971) solved this problem for an instantaneously elastic fluid. Unusual velocity profiles are observed prior to the steady state, due to reflection of the shear wave from the opposite boundary. Zhou, Cook & McKinley (2012) have shown that this behaviour is retained in a set of equations which model start-up Couette flow in a shear-banding fluid. The transmission, reflection and interference of the shear wave lead to the formation of shear bands. Therefore, the equilibrium shear profile ultimately depends upon the start-up motion of the plate, which is a continuous approximation to a Heaviside function.

This paper aims to advance the understanding of the mechanisms of disturbance amplification in viscoelastic liquids. Disturbance evolution in viscoelastic Couette flow is studied by writing the linear perturbation equations as a forced-response problem for the wall-normal vorticity. The forcing is a decaying streamwise vortex, or 'roll', which has an associated cross-flow-plane conformation field. Results consistent with previous work on inertialess transient growth are retrieved as a special case. Furthermore, the implications of the hyperbolic stress evolution equations for transient amplification are demonstrated. A number of limiting forms of the wall-normal vorticity equation are derived, which are used to describe the trends seen in the transient response. It should be cautioned that the analyses presented herein are focused on streamwise elongated disturbances only. The behaviour of oblique modes is not addressed, and cannot necessarily be inferred from the current results (Azaiez & Homsy 1994; Rallison & Hinch 1995).

The rest of this paper is organized as follows. In § 2 the governing linear equations are presented, and are reduced for streamwise-independent disturbances. The dispersion relation of the forcing vortex is discussed in § 3. The solution of the initial value problem which governs the wall-normal vorticity response is presented in § 4, and the various dynamical regimes are discussed. Finally, conclusions are provided in § 5.

2. Theoretical formulation

2.1. *Viscoelastic model and base flow*

On a macroscopic scale, viscoelastic fluids are characterized by their ability to support normal stress differences and their memory of flow history. These properties arise from the tendency of polymers dispersed in the solvent to align themselves with the shear. In such configurations, they are stretched while entropic forces continually act to relax them to their equilibrium, coiled state. In the simplest model, the relaxation of the polymer is captured by a single time scale, ς, which corresponds to modelling a polymer chain as a single spring. The assumption of a linear spring force produces the Oldroyd-B model (Bird, Armstrong & Hassager 1987).

The Oldroyd-B model has several well-known deficiencies. For example, it does not model shear thinning, although this restriction is not severe for dilute solutions and, in particular, Boger fluids which are designed to not exhibit shear thinning (James 2009). In addition, the assumption of a linear spring leads to the prediction of infinite stresses in extensional flows. Where the influence of finite extensibility is important, for example in defining stability boundaries in shear flows, the FENE-P model can be adopted and its prediction matches the Oldroyd-B analysis when the constraint on maximum extensibility is relaxed (Ray & Zaki 2014). However, the Oldroyd-B model includes the physical effect responsible for much of the new dynamics, namely the first normal stress difference. As a result, in certain problems, e.g. the study of melt fracture, the even simpler upper-convected Maxwell model is a good starting point (see Graham 1999; Morozov & Saarloos 2007). Evidence of the adequacy of the Oldroyd-B model is provided by the agreement between linear theory and experiments in inertialess Taylor–Couette flow (Larson, Shaqfeh & Muller 1990). It has also been used to predict the onset of turbulent drag reduction using polymer additives (Min *et al.* 2003), although typically a nonlinear spring law is introduced to avoid unbounded polymer stretch (e.g. Dubief *et al.* 2004; Terrapon *et al.* 2004).

The Oldroyd-B model is used throughout this work, motivated by the desire to assess the role of stress relaxation on streak amplification, without introducing additional physical effects. The total stress tensor is written in terms of a solvent and a polymer contribution. The solvent stress obeys the familiar Newtonian constitutive equations, while the polymer, or elastic, stress is $\mu_p T_{ij} = \mu_p(C_{ij} - \delta_{ij})/\varsigma$. The tensor C_{ij} is the polymer conformation. The equations of motion can then be written as:

$$\frac{\partial U_i}{\partial x_i} = 0, \tag{2.1}$$

$$\rho\left(\frac{\partial U_i}{\partial t} + U_j\frac{\partial U_i}{\partial x_j}\right) = -\frac{\partial P}{\partial x_i} + \mu_s\frac{\partial^2 U_i}{\partial x_j \partial x_j} + \mu_p\frac{\partial T_{ij}}{\partial x_j}, \tag{2.2}$$

$$\overset{\triangledown}{C}_{ij} \equiv \underbrace{\frac{\partial C_{ij}}{\partial t} + U_k\frac{\partial C_{ij}}{\partial x_k}}_{\text{advection}} - \underbrace{C_{ik}\frac{\partial U_j}{\partial x_k} - C_{kj}\frac{\partial U_i}{\partial x_k}}_{\text{stretching/distortion}} = \underbrace{-\frac{1}{\varsigma}(C_{ij} - \delta_{ij})}_{\text{relaxation}}. \tag{2.3}$$

The operator $(\overset{\triangledown}{\cdot})$ is the upper-convected derivative. The choice to write the total stress in terms of solvent and polymer contributions is useful for the interpretation of some of the results in this paper.

It is at times also instructive to consider the fluid as a whole by introducing the total stress, $\sigma_{ij} = 2\mu_s E_{ij} + \mu_p(C_{ij} - \delta_{ij})/\varsigma$. Substituting into (2.3), and using the fact that $\overset{\triangledown}{\delta}_{ij} = -2E_{ij}$, leads to the evolution equation:

$$\varsigma\, \overset{\triangledown}{\sigma}_{ij} + \sigma_{ij} = 2(\mu_s + \mu_p)\left(E_{ij} + \varsigma\beta\, \overset{\triangledown}{E}_{ij}\right). \tag{2.4}$$

This formulation describes the stress (strain rate) response to an applied strain rate (stress). A new time scale, $\varsigma\beta$, emerges, where $\beta = \mu_s/(\mu_s + \mu_p)$ is the ratio of solvent to total viscosity. This time scale is denoted the retardation time, and it captures the degree to which the strain rate remembers the history of stress. For moderate β, an Oldroyd-B fluid describes a dilute polymer solution, and $\beta \to 0$ is a crude model of a polymer melt. If $\beta = 0$, the fluid is said to be instantaneously elastic, or an upper-convected Maxwell fluid.

The base state is steady Couette flow, driven by the relative motion of two plates moving at $\pm U_0$ and separated by a distance $2d$. The Reynolds number is based on the total viscosity, $R = U_0 d/(\nu_s + \nu_p)$. A non-dimensional relaxation parameter, the Weissenberg number, $W = \varsigma U_0/d$, quantifies the ratio between the relaxation and convective time scales.

The non-dimensional base-state velocity field is identical to the Newtonian solution:

$$U = \dot{\gamma} y, \tag{2.5}$$

where the shear rate, $\dot{\gamma} = 1$, has been retained for clarity. This produces the constant polymeric stresses:

$$\boldsymbol{T} = \begin{bmatrix} 2W\dot{\gamma}^2 & \dot{\gamma} & 0 \\ \dot{\gamma} & 0 & 0 \\ 0 & 0 & 0 \end{bmatrix}. \tag{2.6}$$

The equations governing infinitesimal perturbations to this state are presented next and are subsequently restricted to streamwise-independent disturbances. This assumption simplifies the governing dynamical system, while retaining the essential elements to study the development of streaks in this viscoelastic flow configuration.

2.2. *Linear equations: homogeneous and forced-response subsystems*

The equations governing the evolution of small perturbations are:

$$\frac{\partial u_i'}{\partial x_i} = 0, \tag{2.7}$$

$$\frac{\partial u_i'}{\partial t} + U_j \frac{\partial u_i'}{\partial x_j} + u_j' \frac{\partial U_i}{\partial x_j} = -\frac{\partial p'}{\partial x_i} + \frac{\beta}{R} \frac{\partial^2 u_i'}{\partial x_j \partial x_j} + \frac{(1-\beta)}{R} \frac{1}{W} \frac{\partial c_{ij}'}{\partial x_j}, \tag{2.8}$$

$$\frac{\partial c_{ij}'}{\partial t} + U_k \frac{\partial c_{ij}'}{\partial x_k} + u_k' \frac{\partial C_{ij}}{\partial x_k} = C_{ik} \frac{\partial u_j'}{\partial x_k} + c_{ik}' \frac{\partial U_j}{\partial x_k} + C_{kj} \frac{\partial u_i'}{\partial x_k} + c_{kj}' \frac{\partial U_i}{\partial x_k} - \frac{1}{W} c_{ij}', \tag{2.9}$$

where uppercase variables denote the base state, and lowercase variables and primes denote perturbation quantities. The parallel base flow allows for a normal-mode assumption in the streamwise and spanwise directions, such that $\phi'(\boldsymbol{x}, t) = \phi(y, t)\exp[\mathrm{i}(k_x x + k_z z)]$. The disturbances of interest are streamwise elongated streaks, which are strongly amplifying in both Newtonian and viscoelastic shear flows. Therefore, the streamwise wavenumber, k_x, is set equal to zero. This decouples the disturbance eigensystem into two subsystems and removes the dependence on the streamwise normal stress for the other components of the state vector. The decoupling in the linear system has featured in previous studies (Hoda *et al.* 2009; Jovanovic & Kumar 2010, 2011). For example, it was used to derive the scaling of kinetic energy growth with the Weissenberg number in zero-Reynolds-number flows (Jovanovic & Kumar 2010). Here, it will be exploited in order to derive a normal-vorticity equation without any explicit dependence on the polymer conformation field. The corresponding Orr–Sommerfeld (O–S) and Squire equations are:

$$\frac{\partial \psi}{\partial t} - \frac{\beta}{R} \nabla_\perp^2 \psi = \frac{(1-\beta) T_v}{R}, \tag{2.10}$$

$$\frac{\partial \eta}{\partial t} - \frac{\beta}{R} \nabla_\perp^2 \eta = \underbrace{-\mathrm{i} k_z v \dot{\gamma}}_{\text{tilting}} + \frac{(1-\beta) T_\eta}{R}, \tag{2.11}$$

where $\psi = \nabla_\perp^2 v$ and $\eta = \mathrm{i}k_z u$. The symbol $\nabla_\perp^2 \equiv \mathscr{D}^2 - k_z^2$ is the Laplacian in the cross-flow plane, with $\mathscr{D}$ denoting the wall-normal derivative. The stress term in the O–S equation is $T_v = (-k_z^2\mathscr{D}c_{22} - \mathrm{i}k_z(\mathscr{D}^2 + k_z^2)c_{23} + k_z^2\mathscr{D}c_{33})/W$. The new term in the Squire equation, $T_\eta = \mathrm{i}k_z(\mathscr{D}c_{12} + \mathrm{i}k_z c_{13})/W$, is the spanwise variation of the streamwise polymer body force. The evolution equations for T_v and T_η are:

$$\left(\frac{\partial}{\partial t} + \frac{1}{W}\right) T_v = \frac{1}{W}\nabla_\perp^2 \psi, \tag{2.12}$$

$$\left(\frac{\partial}{\partial t} + \frac{1}{W}\right) T_\eta = \frac{1}{W}\nabla_\perp^2 \eta + \underbrace{\frac{\mathrm{i}k_z\dot{\gamma}(\mathscr{D}c_{22} + \mathrm{i}k_z c_{23})}{W}}_{\text{polymer stretch}}. \tag{2.13}$$

Finally, replacing T_v and T_η by (2.10) and (2.11) yields

$$\mathscr{L}\psi \equiv \frac{\partial^2\psi}{\partial t^2} + \left(\frac{1}{W} - \frac{\beta}{R}\nabla_\perp^2\right)\frac{\partial\psi}{\partial t} - \frac{1}{RW}\nabla_\perp^2\psi = 0, \tag{2.14}$$

$$\mathscr{L}\eta \equiv \frac{\partial^2\eta}{\partial t^2} + \left(\frac{1}{W} - \frac{\beta}{R}\nabla_\perp^2\right)\frac{\partial\eta}{\partial t} - \frac{1}{RW}\nabla_\perp^2\eta = \mathscr{F}(y, t), \tag{2.15}$$

which are hereafter referred to as the Orr–Sommerfeld and Squire damped wave equations.

The O–S equation (2.14) is autonomous and admits solutions of the form $v(y, t) = \hat{v}(y)\exp(-\mathrm{i}\omega t)$. With this ansatz, the components of the conformation tensor in the cross-flow plane can be defined fully:

$$\hat{c}_{22} = \frac{2W}{(1 - \mathrm{i}\omega W)}\frac{\mathrm{d}\hat{v}}{\mathrm{d}y}, \quad \hat{c}_{23} = \frac{-W}{\mathrm{i}k_z(1 - \mathrm{i}\omega W)}\left(\frac{\mathrm{d}^2}{\mathrm{d}y^2} + k_z^2\right)\hat{v}, \quad \hat{c}_{33} = \frac{-2W}{(1 - \mathrm{i}\omega W)}\frac{\mathrm{d}\hat{v}}{\mathrm{d}y}. \tag{2.16}$$

The equation for the wall-normal vorticity (2.15) is regarded as a forced-response problem. Such an approach has been applied to the study of boundary layer streaks, where an exact resonance between Orr–Sommerfeld and Squire modes creates a transient response in the wall-normal vorticity, or Klebanoff distortions (Zaki & Durbin 2005). The forcing, $\mathscr{F}(y, t)$, contains both a vorticity tilting and a polymer stretching term, and can now be expressed solely in terms of the wall-normal velocity:

$$\begin{aligned} \mathscr{F}(y, t) &= -\mathrm{i}k_z\dot{\gamma}\left(\frac{\partial}{\partial t} + \frac{1}{W}\right)v + \frac{(1-\beta)}{R}\frac{\mathrm{i}k_z\dot{\gamma}(\mathscr{D}c_{22} + \mathrm{i}k_z c_{23})}{W} \\ &= -\mathrm{i}k_z\dot{\gamma}\left[\underbrace{\left(\frac{1}{W} - \mathrm{i}\omega\right)}_{\text{tilting}} - \underbrace{\frac{(1-\beta)}{R(1-\mathrm{i}\omega W)}\nabla_\perp^2}_{\text{polymer stretch}}\right]\hat{v}\mathrm{e}^{-\mathrm{i}\omega t}. \end{aligned} \tag{2.17}$$

An eigenfunction of the homogeneous v-equation (2.14) which has the appearance of a streamwise vortex is selected for the forcing term. This mode shape is invariant with respect to changes in the elasticity of the fluid. It is applied as forcing in the initial value problem for η, and the flow response is analysed. The choice of the forcing mode is discussed in the following section.

3. Streamwise vortex

In this section, eigensolutions to the autonomous equation for v (2.14) are computed. The evolution of these modes describes the dynamics of the streamwise 'roll' structures. The two time scales in the problem have interesting consequences for the eigenvalue spectrum which are examined. A particular mode shape is then selected to force the normal-vorticity equation (2.15) which governs the formation of the streaks.

3.1. *The dispersion relation for the Orr–Sommerfeld mode*

The solution ansatz, $v(y, t) = \hat{v}(y)\exp(-\mathrm{i}\omega t)$, reduces the homogeneous O–S-type equation (2.14) to a two-point boundary value problem:

$$\frac{\mathrm{d}^2\hat{\psi}}{\mathrm{d}y^2} - \lambda^2\hat{\psi} = 0, \tag{3.1}$$

$$\frac{\mathrm{d}^2\hat{v}}{\mathrm{d}y^2} - k_z^2\hat{v} = \hat{\psi}, \tag{3.2}$$

where λ is given by

$$\lambda^2 = k_z^2 - \mathrm{i}\omega R\frac{(1-\mathrm{i}\omega W)}{(1-\mathrm{i}\omega W\beta)}. \tag{3.3}$$

The temporal eigenvalues are obtained by rearranging (3.3):

$$\omega^{\pm} = -\frac{\mathrm{i}}{2W}\left(\frac{W\beta\kappa^2}{R} + 1 \pm \Phi\right), \tag{3.4}$$

with

$$\Phi(\kappa; R, W, \beta) = \left[\left(1 + \frac{W\beta\kappa^2}{R}\right)^2 - \frac{4W\kappa^2}{R}\right]^{1/2}, \tag{3.5}$$

and $\kappa^2 \equiv k_z^2 - \lambda^2$ is a wavenumber in the cross-flow plane. For a given set of parameters, the mode shape, $\hat{v}(y)$, is associated with two possible complex frequencies, $\omega^{\pm}$, as described by (3.4). This is a consequence of the two time scales of the system: solvent diffusion and polymer relaxation. Two initially identical mode shapes can have different time evolutions, since their respective ω and, as a result, their initial slopes, $\partial_t v$, differ.

The solution for $\hat{\psi}(y)$ can be written in terms of hyperbolic functions:

$$\hat{\psi}(y) = K_1\cosh(\lambda y) + K_2\sinh(\lambda y). \tag{3.6}$$

Introducing this solution on the right-hand side of (3.2), in combination with no-slip/no-penetration boundary conditions, forms an eigenvalue problem for λ which behaves like a wall-normal wavenumber for a given mode. The eigenvalues are solutions to the transcendental equations:

$$\left.\begin{aligned} &\lambda\tanh(\lambda) = k_z\tanh(k_z) && \text{symmetric,}\\ &\lambda\tanh(k_z) = k_z\tanh(\lambda) && \text{anti-symmetric,}\end{aligned}\right\} \tag{3.7}$$

and have associated eigenfunctions,

$$\left.\begin{aligned} &\hat{v}(y) = A_k\cosh(k_z y) + A_\lambda\cosh(\lambda y) && \text{symmetric,}\\ &\hat{v}(y) = \underbrace{B_k\sinh(k_z y)}_{\hat{v}_k} + \underbrace{B_\lambda\sinh(\lambda y)}_{\hat{v}_\lambda} && \text{anti-symmetric,}\end{aligned}\right\} \tag{3.8}$$

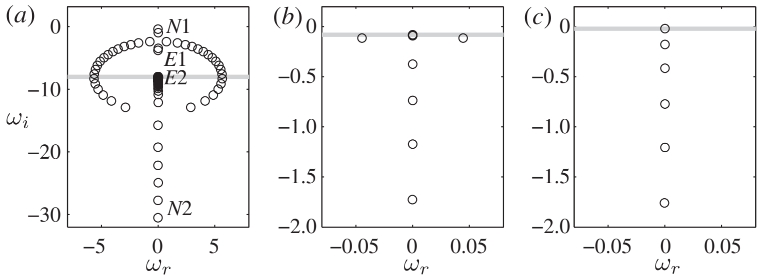

FIGURE 1. Example eigenvalue spectra of the homogeneous O–S-type equation (2.14). Here $R = 25$, $\beta = 0.5$ and $k_z = 1.6$. (*a*) $W = 0.25$, (*b*) $W = 25$, (*c*) $W = 100$. The grey line indicates the retardation rate in each case, $\omega_i = -1/W\beta$. The labels in (*a*) identify limiting forms of ω derived in the text.

where $A_k/A_\lambda = -\lambda \sinh\lambda/k_z \sinh k_z$ and $B_k/B_\lambda = -\lambda \cosh\lambda/k_z \cosh k_z$. Therefore, specification of a spanwise length scale of the disturbance produces the set $\{\lambda_j\}$ with corresponding mode shapes $\{\hat{v}_j(y; \lambda_j)\}$. The other parameters, $\{R, W, \beta\}$, do not alter the mode shapes, namely $\hat{v}_j(y)$ and by continuity $\hat{w}_j(y)$. However, these parameters change the complex frequency of the mode and, as a result, the conformation field in the cross-flow plane (2.16).

Example eigenvalue spectra are shown in figure 1. The spectra have characteristics which distinguish them from their Newtonian counterparts. Most striking are the modes with non-zero frequency, $\omega_r \neq 0$, seen clearly lying in ellipsoidal lobes in figure 1(*a*). Figures 1(*b*) and 1(*c*) show this behaviour diminishing with an increase in elasticity. Figure 1(*a*) has points labelled to identify limiting forms of ω. Consider the first permissible mode shape, $\lambda_j = \lambda_1$, for a given k_z. Its eigenfunction, $\hat{v}(y; \lambda_1)$, has two associated eigenvalues, ω_{N1} and ω_{E1}. For other values of λ_j, $j = 2, 3, \ldots$, the associated eigenvalue pairs move down from $N1$ and up from $E1$. Beyond a particular λ_j, the eigenvalues have non-zero frequency, $\omega^{\pm} = \pm\omega_r + \mathrm{i}\omega_i$. As λ increases, the eigenvalue pairs move down the two ellipsoidal branches until they coalesce again. As the wall-normal wavenumber is increased further, one eigenvalue has a decay rate $\omega_i \to -\infty$, labelled $N2$ on figure 1(*a*). The second eigenvalue approaches a point in the ω-plane, $E2$, leading to an infinite number of modes clustering here. The labelling $N1, 2$ is in reference to a quasi-Newtonian mode and $E1, 2$ denotes an elastic mode. This terminology is explained below and is retained throughout the rest of this paper.

An important parameter appearing in the dispersion relation (3.4) and (3.5) is the ratio of the relaxation time to the disturbance diffusion time scale in the solvent, which we denote Θ:

$$\Theta \equiv \frac{W\beta\kappa^2}{R}. \tag{3.9}$$

The quantity W/R is the elasticity number, which is a ratio of the relaxation and diffusion time scales. An alternative elasticity number can be defined with the solvent viscosity, $E_\beta \equiv \varsigma\nu_s/d^2 = W\beta/R$, in which case $\Theta = E_\beta\kappa^2$ can be interpreted as the product of elasticity and the disturbance wavenumber. It is instructive to consider low- and high-Θ limits of the dispersion relation (3.4). As this is done, the labels from figure 1(*a*) are retained, but the specific locations of these points depend on the parameters chosen. It is also assumed that the solution is sufficiently dilute, such that $(1 - \beta)/\beta = O(1)$. First, consider the case where the polymer relaxes much faster than the rate at which momentum is diffused in the solvent, $\Theta \ll 1$. Then, Φ can be expanded as a power series by assuming Θ as a small parameter, which yields the following approximations to ω:

$$\omega_{N1} \sim -\frac{\mathrm{i}\kappa^2}{R}\left[1+\frac{\Theta(1-\beta)}{\beta}\right], \tag{3.10}$$

$$\omega_{E1} \sim -\frac{\mathrm{i}}{W}\left[1-\frac{\Theta(1-\beta)}{\beta}\right]. \tag{3.11}$$

The first expression is a small correction to the dispersion relation obtained in a Newtonian flow at the same total Reynolds number. In this case, the polymer responds instantaneously and the conformation field results in a polymeric stress proportional to the rate of strain. The polymer therefore behaves as an additional solvent (see (2.16)). The expression for ω_{E1} is a modified relaxation time. In this case, the dynamics are driven by the very large stresses associated with ω_{E1}.

The reciprocal limit is retrieved when the polymer relaxation time is much longer than the solvent diffusion time scale, $\Theta \gg 1$. The expansion of Φ with Θ^{-1} as a small parameter produces the two limiting forms of the dispersion relation:

$$\omega_{E2} \sim -\frac{\mathrm{i}}{W\beta}\left[1+\frac{(1-\beta)}{\beta\Theta}\right], \tag{3.12}$$

$$\omega_{N2} \sim -\frac{\mathrm{i}\beta\kappa^2}{R}\left[1-\frac{(1-\beta)}{\beta\Theta}\right]. \tag{3.13}$$

The first is a modified retardation time for the fluid and results in an infinite number of modes clustered close to this point in the ω-plane. It is associated with polymer stresses of order $\beta/(1-\beta)$ and describes the rate of strain response to a quasi-steady stress. The second approximation, ω_{N2}, describes diffusion in the solvent since the polymer dynamics are frozen with respect to this time scale. The associated conformation field produces a polymer stress $O(1/\Theta) \ll 1$. For sufficiently large $W\beta/R$, any allowable wall-normal wavenumber may result in $\Theta \gg 1$, which is why points $N1$ and $E1$ are eliminated in figure 1(*b*,*c*).

In the region where $\omega_r \neq 0$ (the ellipsoidal region in figure 1*a*) the dynamics of the system cannot be delineated so clearly. This region of the spectrum can be determined from Φ when

$$\frac{2\kappa}{\sqrt{RW}} > \frac{1}{W}+\frac{\beta\kappa^2}{R}. \tag{3.14}$$

This inequality leads to a propagating wave, in contrast to the purely decaying modes discussed above.

The wave propagation can be explained by considering the behaviour of an instantaneously elastic fluid, where $\beta = 0$, $\nu = \nu_p$ and the operator $\tilde{\mathscr{L}} = \mathscr{L}(\beta = 0)$:

$$\tilde{\mathscr{L}} = \mathscr{L}(\beta=0) = \frac{\partial^2}{\partial t^2}+\frac{1}{W}\frac{\partial}{\partial t}-\frac{1}{RW}\nabla_\perp^2. \tag{3.15}$$

This operator is hyperbolic and featured in earlier studies of Stokes' first problem (Preziosi & Joseph 1987). The hyperbolicity is seen in the dispersion relation for (3.15), where there is no upper bound on the region of finite frequency, which occurs when

$$\frac{2\kappa}{M} > \frac{1}{W}. \tag{3.16}$$

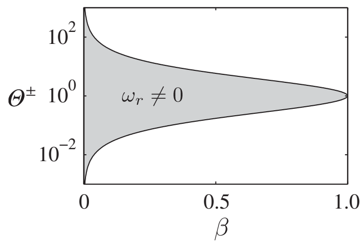

FIGURE 2. Bounds on the region of finite frequency in terms of the relative value of the solvent diffusion and relaxation time scales.

The quantity $M \equiv \sqrt{RW}$ is the viscoelastic Mach number (Joseph 1990) based on the speed of the elastic shear wave $c_s \equiv \sqrt{\nu_p/\varsigma}$. Therefore, the inequality (3.16) states that an eigenmode exhibits a finite phase speed, or equivalently a finite ω_r, if its associated shear wave can travel multiple wavelengths within a relaxation time. As the length scale of the disturbance decreases, the propagation speed in the cross-flow plane tends to the shear wave speed:

$$c_r = \frac{\omega_r}{\kappa} \sim \pm\frac{1}{M}. \tag{3.17}$$

In a more realistic dilute polymer solution with finite β (3.14), this behaviour is curtailed by diffusion in the solvent. The elastic shear wave speed is based on the total viscosity ($c \equiv \sqrt{\nu/\varsigma}$). The parabolic governing equation means this is no longer a well-defined quantity, although it remains helpful in describing the region of finite frequency.

The condition (3.14) encapsulates the requirements for wave propagation. When the length scale of the disturbance is very long ($\kappa \rightarrow 0$), viscous decay is weak, and damping in the system is dominated by the fixed relaxation time. However, the elastic shear wave propagates slowly in relation to the large length scale of the disturbance, so decay is assured. For very short length scales ($\kappa \rightarrow \infty$), the elastic shear wave can propagate many wavelengths of the disturbance within a relaxation time. However, viscous decay in the solvent is very fast, so again damping dominates. The condition of finite frequency defines a region of the parameter space where the length scale of the disturbance is such that neither relaxation nor viscous decay in the solvent can act sufficiently fast to prevent significant propagation of the elastic shear wave.

It is simple to show that this region is centred around, and therefore always includes, the point at which the two time scales (relaxation and solvent diffusion) are exactly equal. The level of disparity required before this behaviour is muted is set by β alone. Considering the bounds defined by (3.14), and solving for the points where the behaviour changes, yields:

$$\Theta^{\pm} = \frac{\pm\beta}{2\sqrt{1-\beta} \pm (2-\beta)}. \tag{3.18}$$

Should $\beta \rightarrow 1$, both bounds tend to unity and the behaviour is lost. The dependence of $\Theta^{\pm}$ on β is shown in figure 2.

Interest in the formation and amplification of streaks focuses attention on eigenmodes of the v-equation (2.14) which resemble streamwise vortices, or ‘rolls’. One such mode shape is shown in figure 3, where the streamlines have the appearance of a row of counter-rotating vortices. Since (2.14) is homogeneous, the vertical

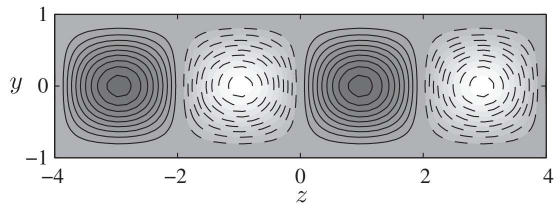

FIGURE 3. Streamlines of the O–S eigenmode in the cross-flow plane. The pattern resembles a streamwise vortex. The mode has a spanwise wavenumber $k_z = 1.6$, which sets $\lambda = -2.63\mathrm{i}$. Dashed lines indicate negative values.

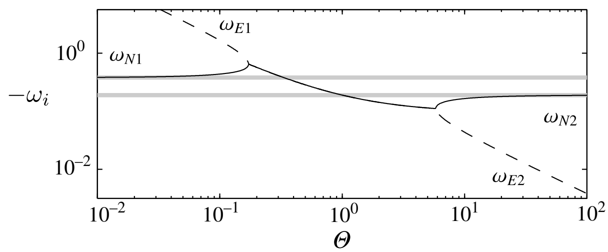

FIGURE 4. The two possible decay rates of the mode approximating a streamwise vortex ($\lambda = -2.63\mathrm{i}$), as a function of the time scale ratio Θ. Horizontal lines are the decay rates of the Newtonian modes at the same total and solvent Reynolds numbers. ——, Described in the text as the quasi-Newtonian mode; – – –, described as the elastic mode. Here $R = 25$, $\beta = 0.5$, $k_z = 1.6$. The labels identify limiting forms of ω described in the text.

velocity, $v(y, t; k_z, \lambda)$, associated with this mode decays exponentially in time. Mass conservation requires that the associated $w(y, t; k_z, \lambda)$ also decays. The particular mode in figure 3 has $k_z = 1.6$, which is the spanwise wavenumber of the optimal disturbance in Newtonian Couette flow (Butler & Farrell 1992). Its wall-normal extent is equal to the domain height and $\lambda = -2.63\mathrm{i}$. Changing the flow parameters, and in particular Θ, does not alter the shape of the vortex, but changes its location in the complex ω-plane.

With the disturbance length scale fixed, the two decay rates associated with this particular O–S mode shape are tracked as a function of Θ in figure 4. In the limit $\Theta \ll 1$, the two eigenvalues approach the Newtonian decay rate, $\omega = \omega_{N1} \sim -\mathrm{i}\kappa^2/R$, and the polymer relaxation time, $\omega = \omega_{E1} \sim -\mathrm{i}/W$, respectively. When $\Theta \gg 1$, one eigenvalue describes viscous decay in the solvent, $\omega = \omega_{N2} \sim -\mathrm{i}\beta\kappa^2/R$, and the other describes the fluid retardation time, $\omega = \omega_{E2} \sim -\mathrm{i}/W\beta$. When $\Theta \sim 1$, the two decay rates are identical and $\omega_r^{\pm} \neq 0$. The well-defined limits of the decay rates motivate the terminology 'quasi-Newtonian' and 'elastic' modes. The quasi-Newtonian mode describes the branch, $\omega_N = \omega(\Theta)$, linking ω_{N1} and ω_{N2}. This is the solid line in figure 4. The elastic mode, ω_E, describes the branch linking ω_{E1} and ω_{E2}; the dashed line in figure 4.

3.2. *Forcing: tilting of mean vorticity versus polymer stretch*

The Squire damped wave equation which describes the transient growth of streaks contains two forcing mechanisms: tilting of mean vorticity and polymer stretch (recall (2.15) and (2.17)). The invariance of the O–S eigenfunction to changes in the elastic

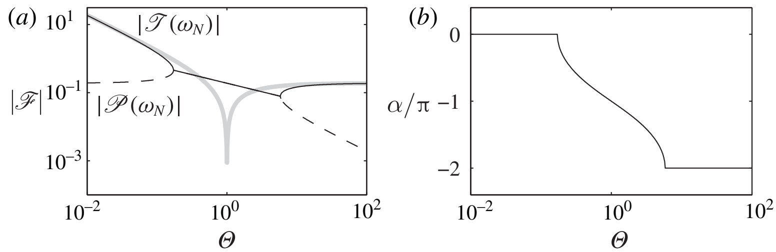

FIGURE 5. (a) A comparison of the size of the forcing terms in the wall-normal vorticity equation as a function of Θ, when forced by the quasi-Newtonian mode: ——, $|\mathscr{T}|$; – – –, $|\mathscr{P}|$; the grey line is the sum, $|\mathscr{T}+\mathscr{P}|$, which acts only on $\hat{v}_\lambda$. (b) $\alpha = \text{phase}(\mathscr{T}) - \text{phase}(\mathscr{P})$ as a function of Θ. $R=25$, $\beta=0.5$.

properties of the fluid means that the wall-normal profiles of the two contributions to $\mathscr{F}$ do not change. However, the magnitude and phase of the initial polymer stresses depend on the complex frequency of the forcing mode. Furthermore, the combined effect of both terms on energy growth is not immediately obvious. Examination of the source term highlights the importance of ω in favouring one mechanism. The forcing term is expressed as:

$$\frac{\mathrm{i}\mathscr{F}(y)}{\dot{\gamma}k_z} = \left[\left(\frac{1}{W} - \mathrm{i}\omega\right) - \frac{(1-\beta)}{R(1-\mathrm{i}\omega W)}\nabla_\perp^2\right]\hat{v} = \underbrace{\mathscr{T}\hat{v}}_{\text{tilting}} + \underbrace{\mathscr{P}\hat{v}_\lambda}_{\text{polymer stretch}}. \tag{3.19}$$

Here, $\mathscr{T} \equiv W^{-1} - \mathrm{i}\omega$ and $\mathscr{P} \equiv \kappa^2(1-\beta)/R(1-\mathrm{i}\omega W)$ describe the coefficients of mean vorticity tilting and polymer stretch, respectively. Note that the polymer stresses are only a function of $\hat{v}_\lambda = A_\lambda \cosh(\lambda y)$, which is the second solution for $\hat{v}$ (see (3.8)).

The magnitudes of the coefficients are plotted in figure 5(a) for the quasi-Newtonian mode, which has a Newtonian decay rate when the diffusion and relaxation time scales differ significantly. The dynamics of the response are set by the relative weightings of the terms in the operator $\mathscr{L}$, but this figure identifies the dominant contribution to the forcing. Vorticity tilting is orders of magnitude larger than polymer stretch for both small and large values of Θ.

The magnitude of the polymer body force term is identical to the vorticity tilting term throughout the finite-frequency region. However, there is a phase difference between the two terms which can suppress the efficacy of tilting. This is captured by the phase angle, $\alpha = \text{phase}(\mathscr{T}) - \text{phase}(\mathscr{P})$, which is plotted in figure 5(b). The two coefficients cancel one another entirely when the two time scales are equal, $\Theta = 1$. The suppression of the lift-up term only applies to one component of the vertical velocity, $\hat{v}_\lambda = A_\lambda \cosh(\lambda y)$. This particular component is the rotational part of the initial condition, since the streamwise vorticity is $\hat{\omega}_x = -\mathrm{i}\kappa^2 A_\lambda \cosh(\lambda y)/k_z$. Therefore, the polymer distortion term acts to suppress the effects of streamwise rotation. The contribution from the irrotational component, $\hat{v}_k = A_k \cosh(k_z y)$, to $\mathscr{F}$ is unaltered throughout by $\mathscr{P}\hat{v}_\lambda$.

Similar to figure 5, the magnitudes of the forcing terms $\mathscr{T}$ and $\mathscr{P}$ and their relative phase are plotted in figure 6 for the elastic mode. The decay rate of this mode tends towards the relaxation and retardation rates in the limits of small and large Θ, respectively. The coefficient of the polymer stretch term for elastic forcing is exactly equal to that of the quasi-Newtonian vortex tilting term: $|\mathscr{P}(\omega_E)| = |\mathscr{T}(\omega_N)|$. The forcing differs in its decay rate and only acts on the second component of the vertical eigenfunction, $\hat{v}_\lambda$.

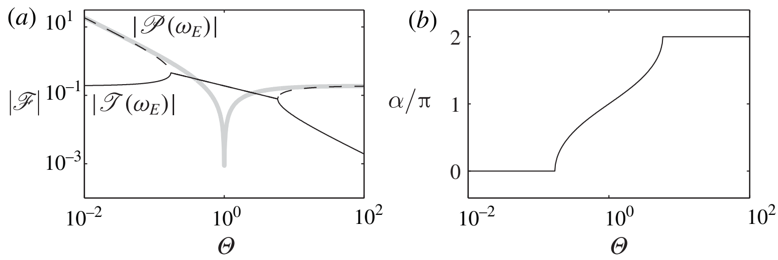

FIGURE 6. (*a*) A comparison of the size of the forcing terms in the wall-normal vorticity equation as a function of Θ, when forced by the elastic mode: ——, $|\mathscr{T}|$; – – –, $|\mathscr{P}|$; the grey line is the sum, $|\mathscr{T}+\mathscr{P}|$, which acts only on $\hat{v}_\lambda$. (*b*) $\alpha = \text{phase}(\mathscr{T}) - \text{phase}(\mathscr{P})$ as a function of Θ. $R=25$, $\beta=0.5$.

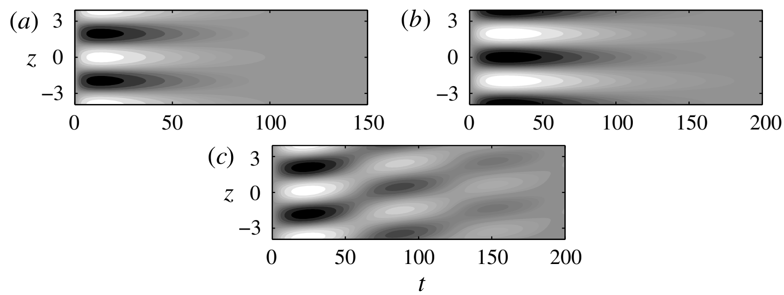

FIGURE 7. Contours of $\text{Re}[u(y=0,t)\exp(\text{i}k_z z)]$, obtained from numerical solution of the initial value problem. (*a*) Forcing from a quasi-Newtonian mode, $\omega=\omega_{N1}$ with $\Theta \ll 1$; $R=100$, $W=0.5$, $\beta=0.5$. (*b*) Forcing from an elastic mode, $\omega=\omega_{E2}$, $\Theta \gg 1$; $R=0.5$, $W=50$, $\beta=0.5$. (*c*) Forcing has non-zero frequency, with $\Theta \sim 1$; $R=50$, $W=50$, $\beta=0.1$.

4. The normal vorticity response

Much like the earlier discussion of the dispersion relation of the O–S modes, the transient normal-vorticity response to forcing by the decaying streamwise vortex can be broadly classified into three categories: (i) quasi-Newtonian, (ii) elastic and (iii) finite-frequency response. These three behaviours are shown in figure 7. Here, and in all subsequent figures, the disturbance has been normalized such that $|v|^2+|w|^2=1$ at $t=0$. The results were obtained from numerical computations of the linearized Navier–Stokes equations, using a Chebyshev expansion in the wall-normal direction and a second-order backward Euler scheme in time. (i) The Newtonian-type behaviour (figure 7*a*) is the response to forcing by the quasi-Newtonian mode. In both the limits $\Theta \ll 1$ and $\Theta \gg 1$, the response has the form of streamwise-independent streaks which amplify in time and subsequently decay. (ii) The elastic-type behaviour (figure 7*b*) is the response to forcing by the elastic mode. In the limit $\Theta \gg 1$, the response is a very slowly decaying, large-amplitude streak, even though the inertia is very weak. This behaviour is consistent with earlier work on transient growth in strongly elastic fluids (Jovanovic & Kumar 2010, 2011). (iii) The most interesting behaviour is seen when $\Theta \sim 1$; an example response is shown in figure 7(*c*). We term this behaviour 're-energization' of the streaks. In this instance, the Squire response resembles a superposition of unequal, counter-propagating waves in the span. Both the asymmetry and the 're-energization' when $\Theta \sim 1$ will be examined in detail in § 4.4.

The physical mechanisms controlling these different transient responses are not evident from the numerical solutions. Therefore, this section focuses on explaining the different dynamical regimes. First, an exact analytical solution to the initial value problem is presented. The solution confirms that it is the value of Θ, and the choice of the forcing O–S mode, that determine the response. Then, the mechanics of the flow are explained using limiting forms of the governing Squire damped wave operator.

4.1. *Solution of the Squire initial value problem*

The wall-normal vorticity response is governed by the inhomogeneous initial-boundary-value problem:

$$\frac{\partial^2\eta}{\partial t^2}+\left(\frac{1}{W}-\frac{\beta}{R}\nabla_\perp^2\right)\frac{\partial\eta}{\partial t}-\frac{1}{RW}\nabla_\perp^2\eta=-\mathrm{i}k_z\dot{\gamma}\left[\left(\frac{1}{W}-\mathrm{i}\omega\right)-\frac{(1-\beta)}{R(1-\mathrm{i}\omega W)}\nabla_\perp^2\right]\hat{v}\mathrm{e}^{-\mathrm{i}\omega t}. \tag{4.1}$$

The second-order differential equation requires two initial conditions, on η and $\partial_t\eta$. The case of zero initial wall-normal vorticity is considered, $\eta(y, t=0)=0$. In addition, c_{12} and c_{13}, which only feature in the Squire sub-system, are also set to zero at initial time. This condition is equivalent to zero initial polymer force in the modified Squire equation, $T_\eta(y, 0)=0$ (see (2.11)), and therefore $\partial_t\eta(t=0)=-\mathrm{i}k_z\dot{\gamma}v(y, t=0)$.

A general solution to (4.1) is found using the Laplace transform. Details are relegated to the Appendix. The solution is most conveniently written in the form:

$$\begin{aligned}\eta(y, t) &= \hat{\eta}_p(y)\mathrm{e}^{-\mathrm{i}\omega t}+\sum_{j=1}^{\infty}C_j(\omega_{\eta,j}^{+}; \omega, R, W, \beta)\cosh(\lambda_{\eta,j}y)\exp(-\mathrm{i}\omega_{\eta,j}^{+}t)\\ &\quad+\sum_{j=1}^{\infty}C_j(\omega_{\eta,j}^{-}; \omega, R, W, \beta)\cosh(\lambda_{\eta,j}y)\exp(-\mathrm{i}\omega_{\eta,j}^{-}t),\end{aligned} \tag{4.2}$$

where the $\cosh(\lambda_{\eta,j}y)$ are the even eigenfunctions of the homogeneous Squire damped wave equation and $\lambda_{\eta,j}=(2j-1)\mathrm{i}\pi/2$ the wall-normal wavenumbers. While the eigenvalues are not equal to those of the forcing O–S mode, they satisfy a dispersion relation of similar form:

$$\omega_{\eta,j}^{\pm}=-\frac{\mathrm{i}}{2W}\left(\frac{W\beta\kappa_{\eta,j}^2}{R}+1\pm\Phi_{\eta,j}\right), \tag{4.3}$$

where $\kappa_{\eta,j}^2=k_z^2-\lambda_{\eta,j}^2$ and

$$\Phi_{\eta,j}(\kappa_{\eta,j}; R, W, \beta)=\left[\left(1+\frac{W\beta\kappa_{\eta,j}^2}{R}\right)^2-\frac{4W\kappa_{\eta,j}^2}{R}\right]^{1/2}. \tag{4.4}$$

Therefore, the asymptotic forms of the dispersion relation found in § 3 are relevant to the transient response as well. The decay rate of the disturbance was demonstrated to have well-defined limiting behaviour with small and large values of Θ. The analytical solution suggests that this may be the same criterion as that which dictates the streak response. However, there are additional factors to consider. The forcing term contains

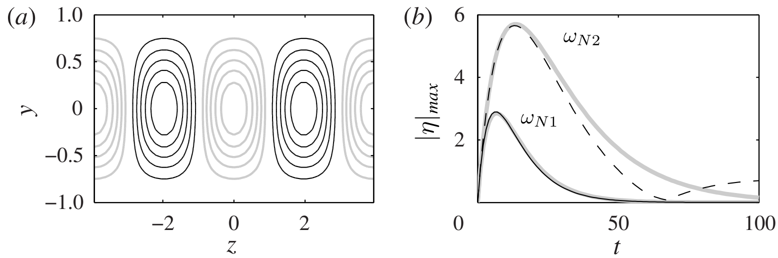

FIGURE 8. Quasi-Newtonian mode. (*a*) Contours of the forcing term in the cross-flow plane, $\mathrm{Re}[\mathscr{F}(y)\exp(\mathrm{i}k_z z)]$, the grey lines indicate negative values. (*b*) The wall-normal vorticity response at $R = 50$, $\beta = 0.5$ in the limit $\Theta \ll 1$ (——), $W = 0.5$, and in the limit $\Theta \gg 1$ (– – –), $W = 300$. The grey lines are the Newtonian solutions at the same total and solvent Reynolds numbers.

the effects of both the vorticity tilting and the polymer stretching terms. It is not clear how their combination affects amplification. Moreover, the mechanism behind the observed re-energization of streaks when $\Theta \sim 1$ is unclear. In order to address these points, solutions to the Squire equation are computed for a range of Θ, and limiting forms of the governing equation are considered in detail.

When assembling the results there is a large parameter space to consider. The situation is muddied further by the two potential forcing modes. To simplify the presentation, we consider the forcing modes separately. First, results are presented for forcing by the quasi-Newtonian mode (§ 4.2). The streaks resulting from forcing by the elastic mode are discussed next (§ 4.3). Finally, the re-energizing streaks are explained (§ 4.4). These structures occur when $\Theta \sim 1$, and the terminology of 'quasi-Newtonian' and 'elastic' modes is no longer appropriate, since both forcing modes have identical decay rates.

4.2. *The quasi-Newtonian mode*

The term quasi-Newtonian mode is applicable when there is a large disparity between the relaxation and solvent diffusion time scales, since the modal decay rate approaches a Newtonian value in the limits $\Theta \ll 1$ and $\Theta \gg 1$. The structure of the forcing, $\mathscr{F}$, due to the quasi-Newtonian mode is shown in figure 8(*a*). The forcing term resembles a streamwise vortex, consistent with the assessment in § 3.2 of the dominant contribution to the forcing term. Figure 8(*b*) shows the amplitude of the resulting streaks in both the low- and high-Θ limits, where the response is observed to be very close to the Newtonian curves. The latter were computed at the same total and solvent Reynolds numbers, respectively. Recovering Newtonian behaviour from the governing equation is made easier by rescaling time, $\tilde{t} = t\beta\kappa^2/R$ with $\tilde{\eta}(y, \tilde{t}) = \eta(y, t)$, to reflect that the decay rate of the forcing term is set by a viscous time scale. After rearrangement, the governing equation reads:

$$\frac{W\beta\kappa^2}{R}\frac{\partial^2\tilde{\eta}}{\partial\tilde{t}^2} + \left(1 - \frac{W\beta}{R}\nabla_\perp^2\right)\frac{\partial\tilde{\eta}}{\partial\tilde{t}} - \frac{1}{\beta\kappa^2}\nabla_\perp^2\tilde{\eta} = \hat{f}(y)\exp(-\mathrm{i}\omega R\tilde{t}/\beta\kappa^2). \tag{4.5}$$

Fast polymer relaxation: If the polymer relaxes much faster than solvent diffusion, then the appropriate small parameter is $\epsilon = \Theta \ll 1$. The equation becomes:

$$\epsilon\frac{\partial^2\tilde{\eta}}{\partial\tilde{t}^2} + \left(1 - \frac{\epsilon}{\kappa^2}\nabla_\perp^2\right)\frac{\partial\tilde{\eta}}{\partial\tilde{t}} - \frac{1}{\beta\kappa^2}\nabla_\perp^2\tilde{\eta} = \hat{f}(y; \epsilon)\exp(-\mathrm{i}\omega_{N1}R\tilde{t}/\beta\kappa^2). \tag{4.6}$$

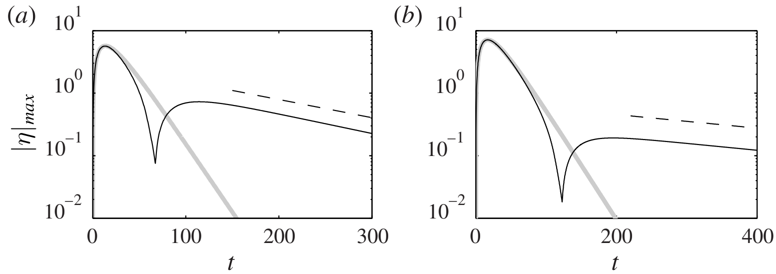

FIGURE 9. Quasi-Newtonian mode with large Θ. Grey lines are the Newtonian solutions at the same solvent Reynolds numbers. Black line is the exact solution. (*a*) $\Theta \sim 30$, with $R=50$, $W=300$, $\beta=0.5$; (*b*) $\Theta \sim 40$, with $R=100$, $W=500$, $\beta=0.8$. The dashed lines identify the retardation rate, $\eta \propto -t/W\beta$.

In this limit, the appropriate approximation for ω has been adopted ($\omega = \omega_{N1} \sim -\mathrm{i}\kappa^2/R$). Note that this approximation assumed a relatively dilute polymer solution, $(1-\beta)/\beta = O(1)$. Neglecting terms of $O(\epsilon)$ in the forcing, the right-hand side reduces to the familiar forcing term from the Newtonian Squire equation, $\hat{f}(y;\ \epsilon) \sim -\mathrm{i}k_z\dot{\gamma}R\hat{v}\exp(-\tilde{t}/\beta)/\beta\kappa^2$. Therefore, assuming an asymptotic expansion $\tilde{\eta} = \tilde{\eta}_0 + \epsilon\tilde{\eta}_1 + \cdots$, at leading order the wall-normal vorticity equation is:

$$\frac{\partial \tilde{\eta}_0}{\partial \tilde{t}} - \frac{1}{\beta\kappa^2}\nabla_\perp^2\tilde{\eta}_0 = -\mathrm{i}k_z\dot{\gamma}\frac{R}{\beta\kappa^2}\hat{v}\mathrm{e}^{-\tilde{t}/\beta}. \tag{4.7}$$

Reverting back to the convective time scale reveals that the governing equation is simply the Newtonian Squire equation at the same total Reynolds number. This is expected since the polymer can effectively respond instantaneously on a solvent time scale. The presence of a small parameter in front of the leading-order derivative does not lead to boundary-layer-type behaviour, since the leading-order equation satisfies the initial conditions exactly.

Slow polymer relaxation: The response due to the quasi-Newtonian mode when relaxation is much slower than solvent diffusion is considered by introducing $\delta = \Theta^{-1} \ll 1$. The forcing decay rate can then be approximated as $\omega = \omega_{N2} \sim -\mathrm{i}\beta\kappa^2/R$. The wall-normal vorticity equation (4.5) becomes:

$$\frac{\partial^2\tilde{\eta}}{\partial\tilde{t}^2} + \left(\delta - \frac{1}{\kappa^2}\nabla_\perp^2\right)\frac{\partial\tilde{\eta}}{\partial\tilde{t}} - \frac{\delta}{\kappa^2}\nabla_\perp^2\tilde{\eta} = \hat{f}(y;\ \delta)\exp(-\mathrm{i}\omega_{N2}R\tilde{t}/\beta\kappa^2). \tag{4.8}$$

The response in this limit is examined over a long time in figure 9. The streaks are observed to match the Newtonian solution at the same solvent Reynolds number for short times. At longer times a second, much weaker streak amplifies and subsequently decays at the retardation rate, $-1/W\beta$. The second streak can be established as a delayed polymer response. To demonstrate this effect, we introduce the expansion $\tilde{\eta} = \tilde{\eta}_0 + \delta\tilde{\eta}_1 + \cdots$ in (4.8), and retain the equations governing the leading- and first-order terms. These equations are integrated once in time. The original initial conditions are applied at leading order, and homogeneous initial conditions are enforced for $\tilde{\eta}_1$ and its time derivative, which yields:

$$\frac{\partial \tilde{\eta}_0}{\partial \tilde{t}} - \frac{1}{\kappa^2}\nabla_\perp^2\tilde{\eta}_0 = -\mathrm{i}k_z\dot{\gamma}\frac{R}{\beta\kappa^2}\hat{v}\mathrm{e}^{-\tilde{t}}, \tag{4.9}$$

$$\begin{aligned}\frac{\partial \tilde{\eta}_1}{\partial \tilde{t}} - \frac{1}{\kappa^2}\nabla_\perp^2 \tilde{\eta}_1 = {} & \frac{(1-\beta)}{\beta\kappa^2}\int_0^{\tilde{t}} \nabla_\perp^2 \tilde{\eta}_0(y,\sigma)\mathrm{d}\sigma \\ & + \mathrm{i}k_z\dot{\gamma}\frac{R}{\beta\kappa^2}\frac{(1-\beta)}{\beta}\left(1+\frac{1}{\kappa^2}\nabla_\perp^2\right)\left(1-\mathrm{e}^{-\tilde{t}}\right)\hat{v}. \end{aligned} \tag{4.10}$$

The leading-order dynamics are governed by the Newtonian Squire equation for the solvent. This result is understood by considering that (i) the initial polymer stresses are $\ll 1$ (see § 3) and (ii) the polymer is effectively frozen with respect to the time scale of the streamwise roll. At first order, there are new, unfamiliar amplification mechanisms on the right-hand side of (4.9). The term involving $\hat{v}$ is the $O(\delta)$ contribution from polymer stretch in the original forcing term on the right-hand side of (4.1). The integral term is a polymer memory effect. It is a release of energy stored by the polymer after it has been stretched by the initial row of streaks in the solvent. This term is shown below to contribute to the delayed amplification of the streaks seen in figure 9.

In order to capture the long-time behaviour of the streaks, time is now rescaled by relaxation, $T = t/W$, in the full force-response equation. Setting $\eta(y, t) = \overline{\eta}(y, T)$, the governing equation reads:

$$\begin{aligned}& \delta\frac{\partial^2\overline{\eta}}{\partial T^2} + \left(\delta - \frac{1}{\kappa^2}\nabla_\perp^2\right)\frac{\partial\overline{\eta}}{\partial T} - \frac{1}{\beta\kappa^2}\nabla_\perp^2\overline{\eta} \\ & \quad = -\mathrm{i}k_z\dot{\gamma}\frac{R}{\beta\kappa^2}\left[1 - \frac{1}{\delta}\left(1 - \frac{(1-\beta)}{\beta}\delta\right) + \frac{(1-\beta)}{\beta\kappa^2}\nabla_\perp^2 + O(\delta)\right]\hat{v}\mathrm{e}^{-T/\delta}. \end{aligned} \tag{4.11}$$

Equation (4.11) has a boundary layer of thickness $T \sim \Theta^{-1}$, where the solution matches the faster dynamics discussed above in relation to the solvent time scale. If, however, we consider the behaviour on the slow time scale, at leading order equation (4.11) reduces to:

$$\left(\frac{\partial}{\partial T} + \frac{1}{\beta}\right)\nabla_\perp^2\overline{\eta}_0 = 0. \tag{4.12}$$

The solution to (4.12) is $\overline{\eta}_0 = \overline{N}_0(y)\exp(-T/\beta)$. The y-dependence is found by matching the solution $\overline{\eta}(y, T)$ with $\tilde{\eta}(y, \tilde{t})$ as $T \to 0$ and $\tilde{t} \to \infty$. The leading-order solution on the solvent time scale, $\tilde{\eta}_0(y, \tilde{t})$, decays to zero as $\tilde{t} \to \infty$. Therefore, $\overline{N}_0(y) = 0$ and there is no second streak at leading order.

The first-order correction satisfies an identical equation to the leading-order solution (4.12); the solution is again simply $\overline{\eta}_1 = \overline{N}_1(y)\exp(-T/\beta)$. However, at first order the equation on the solvent time scale (4.9) has a non-trivial, steady solution, which yields the function $\overline{N}_1(y)$:

$$\nabla_\perp^2\overline{N}_1 = -\frac{(1-\beta)}{\beta}\int_0^\infty \nabla_\perp^2\tilde{\eta}_0\mathrm{d}\tilde{t} + \mathrm{i}k_z\dot{\gamma}\frac{R}{\beta}\frac{(1-\beta)}{\beta}\left(1+\frac{1}{\kappa^2}\nabla_\perp^2\right)\hat{v}. \tag{4.13}$$

At long time, the decay rate of $\overline{\eta}_1$ is set by the retardation time, which is consistent with the reappearance of the streaks being a release of energy by the polymers back into the flow. Decay at the retardation rate is a characteristic associated with a rate-of-strain response to an applied stress.

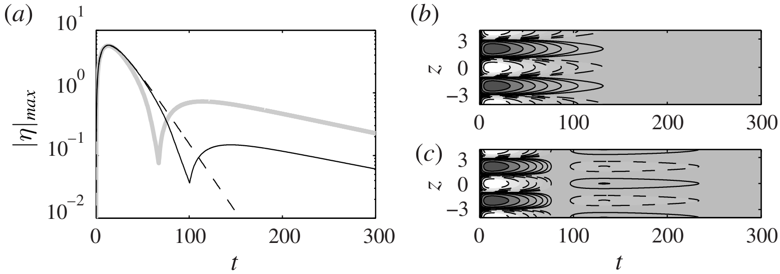

FIGURE 10. First-order correction for large Θ. Here $\Theta \sim 30$, $R = 50$, $W = 300$, $\beta = 0.5$. (*a*) Full solution shown with the thick grey line; – – –, leading-order solution; ——, the composite solution $\tilde{\eta}_0 + \delta(\tilde{\eta}_1 + \overline{\eta}_1 - \overline{N}_1)$. (*b*) Contours of $\mathrm{Re}[u(y = 0, t)\exp(\mathrm{i}k_z z)]$ when forcing is only due to the term involving $\hat{v}$. (*c*) Contours of $\mathrm{Re}[u(y = 0, t)\exp(\mathrm{i}k_z z)]$ when forcing is only due to the memory term.

Figure 10(*a*) shows the composite solution, $\tilde{\eta}_0 + \delta(\tilde{\eta}_1 + \overline{\eta}_1 - \overline{N}_1)$, for an example set of parameters. The first-order correction qualitatively describes the re-emergence of the streaks after their initial decay, but under-predicts their amplitude. The correction also shows that the emergent streaks have an opposite sign to those from the leading-order response. For this reason, the amplitude of the exact solution falls off more quickly than the leading-order approximation after the initial peak. The second, weaker streak has a decay rate set by the retardation time, which explains the second peak in the wall-normal vorticity amplitude at longer time when the leading-order behaviour has decayed.

The emergent streaks are due to the two forcing terms appearing at first order, (4.9). In order to isolate their respective impact, the linearity of the operator is exploited and the equation is solved with forcing from each term separately. Recall that the term associated with $\hat{v}$ is a polymer stretch contribution, the integral term is a polymer memory effect. The solutions associated with forcing by these mechanisms alone are identified with superscripts $\tilde{\eta}^v$ and $\tilde{\eta}^m$. The term involving $\hat{v}$ serves to reinforce the leading-order streaks, as shown in figure 10(*b*), which corresponds to the solution $\tilde{\eta}_0 + \delta(\tilde{\eta}_1^v + \overline{\eta}_1^v - \overline{N}_1^v)$. The polymer-memory term results in the reappearance of the streaks and dominates at long time. This behaviour is plotted in figure 10(*c*), where the contours of $u(y = 0, z, t)$ were extracted from the solution $\tilde{\eta}_0 + \delta(\tilde{\eta}_1^m + \overline{\eta}_1^m - \overline{N}_1^m)$. The streaks resulting from the polymer-memory forcing term are seen for $t > 100$.

Since the transient streak growth follows the Newtonian curve at the same solvent Reynolds number, a large R/β is required for the streaks to reach a significant amplitude. In turn, this requires large W to ensure $\Theta \gg 1$, as shown in figures figures 9 and 10. It should be cautioned that the Oldroyd-B model becomes increasingly unrealistic as the Weissenberg number is increased, because it neglects the finite extensibility of the polymers. Therefore, future work must assess the influence of finite extensibility on streak amplification in this regime.

4.3. *The elastic mode*

The terminology 'elastic mode' describes the branch $\omega(\Theta)$ which is set by the polymer time scale when the diffusion and relaxation time scales are disparate. In this case, the forcing term in the Squire damped wave equation is dominated by polymer stretching rather than tilting of mean vorticity, as previously shown in

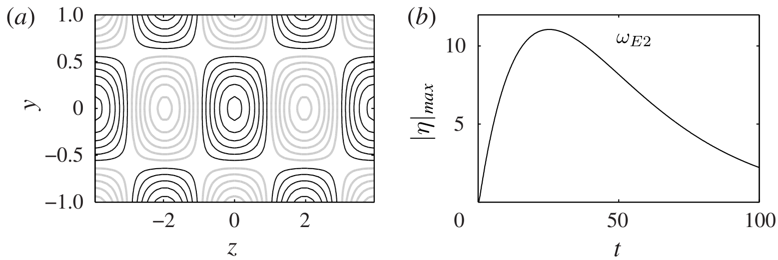

FIGURE 11. Elastic mode. (a) Contours of the forcing term in the cross-flow plane, $\mathrm{Re}[\mathscr{F}(y)\exp(\mathrm{i}k_z z)]$, the grey lines indicate negative values. (b) The wall-normal vorticity response in the limit $\Theta \gg 1$. The parameters are $W = 50$, $R = 0.5$, $\beta = 0.5$.

figure 6(a). Attention will be focused on the case where $\Theta \gg 1$, and no results are shown for $\Theta \ll 1$. In the latter limit, the streak response to forcing by an elastic O–S mode is always significantly weaker than the response to a quasi-Newtonian O–S mode, at the same parameters. This observation is intuitive because the limit $\Theta \ll 1$ implies $W \ll R/\beta\kappa^2$, and since $\omega_{E1} \sim -\mathrm{i}/W$ and $\omega_{N1} \sim -\mathrm{i}\kappa^2/R$, the decay rate of the elastic O–S forcing is rapid compared to the quasi-Newtonian case.

Results for $\Theta \gg 1$ are shown in figure 11 and were computed using numerical solution of the linearized disturbance equations. Contours of the total forcing term from an elastic O–S mode are plotted in a cross-flow plane figure 11(a). The wall-normal vorticity response is shown in figure 11(b): despite the very weak inertia, the streak reaches a significant amplitude over a long time scale.

The mechanics of the response are not clear at first sight, so an approximate form of the wall-normal vorticity equation is sought for the elastic mode when $\delta^{-1} = \Theta \gg 1$. The decay of the forcing is set by the fluid's elastic properties, so time is rescaled accordingly, $T = t/W$, with $\overline{\eta}(y, T) = \eta(y, t)$. The Squire damped wave equation then takes the form:

$$\delta \frac{\partial^2 \overline{\eta}}{\partial T^2} + \left(\delta - \frac{1}{\kappa^2}\nabla_\perp^2\right)\frac{\partial \overline{\eta}}{\partial T} - \frac{1}{\beta\kappa^2}\nabla_\perp^2 \overline{\eta} = \frac{WR}{\beta\kappa^2}\mathscr{F}(y)\mathrm{e}^{-T/\beta}. \tag{4.14}$$

At leading order:

$$\left(\frac{\partial}{\partial T} + \frac{1}{\beta}\right)\nabla_\perp^2 \overline{\eta}_0 = \mathrm{i}k_z\dot{\gamma}W\nabla_\perp^2\hat{v}\mathrm{e}^{-T/\beta}. \tag{4.15}$$

The solution can be written in the form:

$$\overline{\eta}_0(y, T) = \mathrm{i}k_z\dot{\gamma}W\hat{v}\,T\mathrm{e}^{-T/\beta} + N_0(y)\mathrm{e}^{-T/\beta}. \tag{4.16}$$

The solution (4.16) demonstrates that streak growth follows $\eta \propto t\exp(-t/W\beta)$: the amplitude is proportional to time but ultimately decays due to the retardation rate. This result is in agreement with the work on inertialess transient growth in Jovanovic & Kumar (2010). Note that in (4.16), the first term on the right-hand side is independent of Reynolds number. Therefore, as $R \to 0$, the large growth of the streaks is retained.

Since (4.14) is first order in time, it is not possible to impose both initial conditions. Instead, the function $N_0(y)$ can be determined by matching the outer dynamics to an inner solution. Indeed, (4.14) has a boundary layer of thickness $T \sim \Theta^{-1}$ at $T = 0$

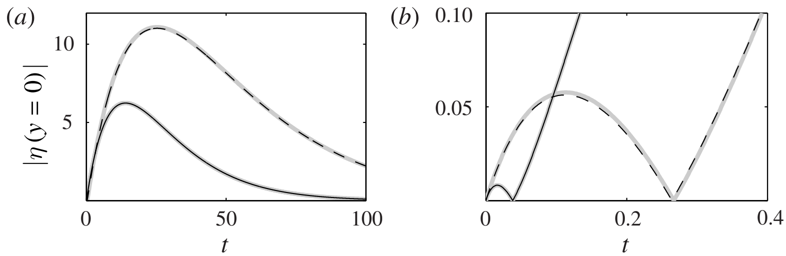

FIGURE 12. (*a*) Comparison of the numerical and asymptotic solutions with elastic forcing in the limit $\varTheta \gg 1$. Grey lines are the numerical solutions; ——, $\varTheta = 1327$, with $R = 0.1$, $W = 20$, $\beta = 0.7$; – – –, $\varTheta = 474$, with $R = 0.5$, $W = 50$, $\beta = 0.5$. (*b*) The short-time behaviour.

where the dynamics of the solvent are dominant. Rescaling $\tilde{t} = T/\delta \equiv t\beta\kappa^2/R$, with $\tilde{\eta}(y, \tilde{t}) = \overline{\eta}(y, T)$, we find, at leading order:

$$\frac{\partial}{\partial \tilde{t}}\left(\frac{\partial \tilde{\eta}_0}{\partial \tilde{t}} - \frac{1}{\kappa^2}\nabla_\perp^2 \tilde{\eta}_0\right) = \mathrm{i}k_z\dot{\gamma}\frac{R}{\beta\kappa^2}\hat{v}_\lambda. \tag{4.17}$$

Integration and application of the scaled initial condition $\partial_{\tilde{t}}\tilde{\eta}(\tilde{t} = 0) = -\mathrm{i}k_z\dot{\gamma}R\hat{v}/\beta\kappa^2$ reveals the short-time dynamics are governed by:

$$\frac{\partial \tilde{\eta}_0}{\partial \tilde{t}} - \frac{1}{\kappa^2}\nabla_\perp^2 \tilde{\eta}_0 = -\mathrm{i}k_z\dot{\gamma}\frac{R}{\beta\kappa^2}\hat{v} + \mathrm{i}k_z\dot{\gamma}\frac{R}{\beta\kappa^2}\hat{v}_\lambda\tilde{t}. \tag{4.18}$$

This is the Newtonian Squire equation at the solvent Reynolds number. A solution using Laplace transforms is presented in the appendix. It is matched to the outer solution (4.16) to determine the function $N_0(y)$. A uniformly valid composite solution can therefore be written in the form:

$$\eta_0(y, t) = \mathrm{i}k_z\dot{\gamma}\hat{v}(y)t\mathrm{e}^{-t/W\beta} + N_0(y)\mathrm{e}^{-t/W\beta} + \sum_{j=1}^{\infty} S_j(\omega_{\eta,j}; R, \beta)\cosh(\lambda_{\eta,j}y)\exp(-\mathrm{i}\omega_{\eta,j}t), \tag{4.19}$$

where $\omega_{\eta,j} = -\mathrm{i}\beta\kappa_{\eta,j}^2/R$ are the homogeneous Squire eigenvalues due to the solvent. A comparison of the asymptotic solutions with the numerical results is shown in figure 12. The zoomed-in view in figure 12(*b*) exposes the short time decay of the contribution from the solvent Squire modes. The overall, or long-time, dynamics (figure 12*a*) are dictated by the outer solution (4.16), and clearly show streak growth, even in the inertialess limit.

4.4. *Streak re-energization*

When the relaxation and solvent diffusion time scales are commensurate, $\varTheta \sim 1$, a distinction into quasi-Newtonian and elastic modes is no longer appropriate. This is due to the equal decay rates of the pair of O–S modes with the same eigenfunction, $\mathrm{Im}(\omega^+) = \mathrm{Im}(\omega^-)$. Furthermore, the modes have equal and opposite frequencies, $\mathrm{Re}(\omega^+) = -\mathrm{Re}(\omega^-)$, which introduces some choice in the type of O–S roll used to force the Squire equation. For example, forcing with ω^+ alone corresponds to a row

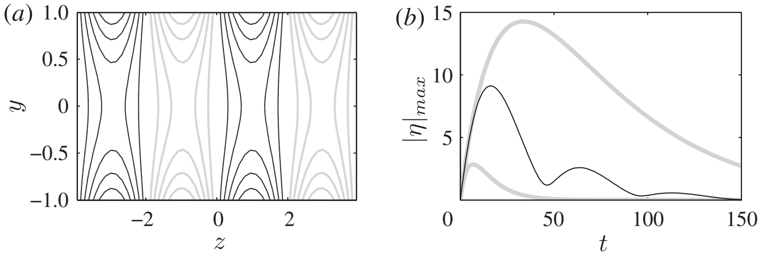

FIGURE 13. Forcing mode has a non-zero frequency. (a) Contours of the forcing term in the cross-flow plane, $\mathrm{Re}[\mathscr{F}(y)\exp(\mathrm{i}k_z z)]$, the grey lines indicate negative values. (b) The wall-normal vorticity response with $\Theta \sim 1$. The parameters are $R=50$, $W=25$, $\beta=0.2$. The grey lines show the Newtonian solutions at same total and solvent Reynolds numbers.

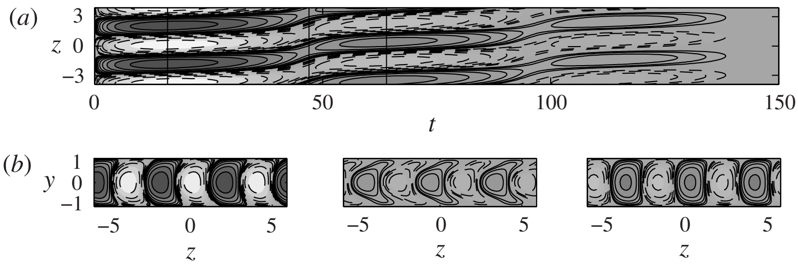

FIGURE 14. (a) Contours of streamwise velocity at the centreline, $\mathrm{Re}[u(y=0,t)\exp(\mathrm{i}k_z z)]$, and ($b$) in the cross-flow plane at times indicated by vertical black lines in (a). Here $\Theta=0.95$; $R=50$, $W=25$, $\beta=0.2$.

of streamwise vortices propagating in the $+z$ direction with speed $|\mathrm{Re}(\omega)|/k_z$. This propagation is only by virtue of the elastic properties of the fluid and is absent in simple Newtonian Couette flow. The disturbance energy of the rolls in this case is monotonically decreasing in time. On the other hand, forcing can be constructed from a superposition of ω^+ and ω^- to form a vortex which pulsates in place. In this instance, the disturbance energy is oscillatory inside a decay envelope. Throughout this section we will compute the response to a single propagating mode, before discussing the properties of the solution due to forcing from a stationary vortex.

When the forcing is due to a single O–S mode, say $\omega=\omega^+$, the forcing term and Squire response are shown in figure 13. As demonstrated in § 3.2, when $\Theta \sim 1$, the polymer conformation field associated with the rolls mutes the rotational component of the tilting term on the right-hand side of the wall-normal vorticity equation. A consequence of this cancellation is that the source term is localized near the walls of the channel, as shown in figure 13(a). Nonetheless, the amplitude of the streak response is enhanced compared with the Newtonian case at the same total Reynolds number (figure 13b).

Although the strength of the normal-vorticity response is enhanced in this regime, the most striking feature of the solution when $\Theta \sim 1$ is the multiple maxima seen in the streak amplitude, $|\eta|_{max}$. This behaviour is explored further in figure 14. Contours of the streamwise velocity perturbation field at the centreline, $u'(y=0, z, t)$, are reported in figure 14(a). The response is a spanwise row of streaks which grow and subsequently decay. Streak decay is accompanied by a shift in the span before the

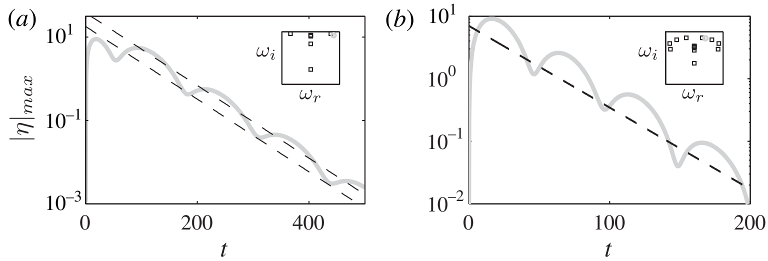

FIGURE 15. Maximum amplitude in the wall-normal vorticity response as a function of time. The dashed lines identify the amplitude of the first even wall-normal vorticity mode pair in the response ($\omega^{\pm}_{\eta,j=1}$). (*a*) $\Theta = 5.69$, with $R = 50$, $W = 100$, $\beta = 0.3$. (*b*) $\Theta = 0.95$, with $R = 50$, $W = 25$, $\beta = 0.2$. The inset shows the (even) spectrum of the wall-normal vorticity operator, with the forcing mode plotted in grey.

cycle of amplification and decay repeats. The streamwise velocity perturbation field in the cross-flow plane at three instances in this process is shown in figure 14(*b*). The streaks fill the channel, but their spanwise shape is asymmetric.

The normal-vorticity response plotted in figure 14 resembles a superposition of unequal, counter-propagating waves in the span. This behaviour was also remarked on in connection with figure 7(*c*), and can be understood in the context of the exact solution (4.2): when $\Theta \sim 1$, the ω_η spectrum of the Squire equation includes finite-frequency modes, and a given eigenfunction is associated with two waves, $\omega^{\pm}_{\eta,j}$, propagating in $\pm z$ with speed $|\mathrm{Re}(\omega_{\eta,j})|/k_z$. The amplitude of the excited Squire modes was given by $C_j \propto (\omega - \omega^{\pm}_{\eta,j})^{-1}$ in (4.2). Since the forcing is from a travelling vortex, say $\omega = \omega^+$, Squire modes travelling in the same direction will be preferentially excited, $C_j(\omega^+_{\eta,j}) > C_j(\omega^-_{\eta,j})$. The solution also contains a wave travelling at the speed of the forcing, $\mathrm{Re}(\omega^+)/k_z$, identified with $\hat{\eta}_p(y)$ in (4.2). The superposition of unequal travelling waves leads to the broken spanwise symmetry in the response (figure 14*a*). This behaviour is affirmed in figure 15, where the amplitudes of the pair of Squire modes with the largest coefficients are overlayed on the full solution. The inset in this figure shows the spectrum of the homogeneous wall-normal vorticity equation, including the location of the forcing O–S mode.

The above perspective includes the wall-normal variation in the response implicitly as a summation of eigenfunctions. This approach does not fully characterize the re-energization process. For this purpose, an appropriate limiting form of the Squire damped wave equation is sought. The relevant time scale is the frequency of the forcing, which, when $\Theta = 1$ exactly, has the form:

$$\mathrm{Re}(\omega^{\pm}) = \pm\frac{\kappa\sqrt{1-\beta}}{\sqrt{RW}}. \tag{4.20}$$

The frequency is inversely proportional to the viscoelastic Mach number, $M \equiv \sqrt{RW}$, and for lower values of β can be approximated as $\mathrm{Re}(\omega^{\pm}) \approx \pm\kappa/\sqrt{RW}$. Using this frequency to define a new time variable, $\hat{t} = t\kappa/\sqrt{RW}$, the Squire damped wave equation becomes:

$$\frac{\partial^2\eta}{\partial\hat{t}^2} + \sqrt{\frac{\beta}{\Theta}}\left(1 - \frac{\Theta}{\kappa^2}\nabla^2_\perp\right)\frac{\partial\eta}{\partial\hat{t}} - \frac{1}{\kappa^2}\nabla^2_\perp\eta = \frac{WR}{\kappa^2}\mathscr{F}(y)\exp(-\mathrm{i}\omega\hat{t}\sqrt{RW}/\kappa). \tag{4.21}$$

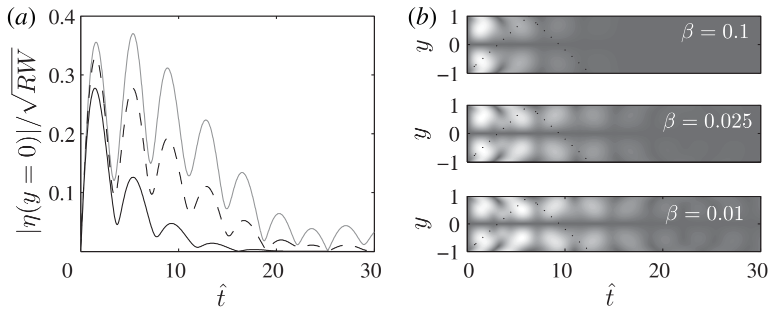

FIGURE 16. (*a*) Wall-normal vorticity amplitude at the centreline for constant Θ with varying β. Here $\Theta = 0.95$, $R = 5$: ——, $W = 5$, $\beta = 0.1$; – – –, $W = 20$, $\beta = 0.025$; grey line, $W = 50$, $\beta = 0.01$. (*b*) Contours of $|\partial\eta/\partial y|$ for the three cases, the dotted lines identify the trajectory of a shear wave.

The normal vorticity response at the centreline is plotted for three $\{W, \beta\}$ pairs, with Θ held constant, in figure 16. The amplitude scales approximately with $\sqrt{RW}$. Re-energization is more evident as the solvent viscosity is reduced, and in the limit $\beta \ll 1$ with $\Theta \sim 1$, the Squire equation (4.21) becomes a forced wave equation in the y–z plane without damping. This suggests that re-energization is a superposition of trapped vorticity waves.

We can connect this understanding to the earlier discussion of the eigenfunction expansion. The forcing term in (4.21) appears oscillatory but is in fact a travelling wave in the span prior to the normal-mode assumption that was invoked in the z-direction. Therefore, the vertical-vorticity response will include a wave travelling in the $+z$-direction with speed $c_z = \mathrm{Re}(\omega^+)/k_z$, which is consistent with the exact solution (4.2). The response also includes vertical-vorticity waves propagating in the cross-flow plane with speed $1/M$. These vorticity waves are reflected from the walls, which act as a waveguide for the counter-propagating waves. An attempt to identify wall-normal wave propagation and reflection is presented in figure 16(*b*), where contours of $|\partial\eta/\partial y|$ are shown. In all cases, identification of wave fronts is difficult due to the smoothing effect of the small but finite solvent viscosity.

The smoothing effect can be removed by considering an instantaneously elastic fluid with $\beta = 0$. To connect the results to the above discussion of $\Theta \sim 1$ we must retain $\epsilon = R/W\kappa^2 \ll 1$. For the instantaneously elastic fluid, the dispersion relation of the forcing takes the form:

$$\omega^{\pm} \sim -\frac{\mathrm{i}}{2W} \pm \frac{\kappa}{M}\left(1 - \frac{\epsilon}{8} + \cdots\right). \tag{4.22}$$

The decay rate of the roll is set by the relaxation time, and the same is true of the excited Squire modes, $\mathrm{Im}(\omega^{\pm}_{\eta,j}) = -1/2W \forall j$. Therefore, the role of polymer relaxation is to set a decay envelope for the response, and the wall-normal vorticity can be written in the form $\eta(y, t) = \tilde{\eta}(y, t)\exp(-t/2W) = \tilde{\eta}(y, \hat{t})\exp(-\sqrt{\epsilon}\hat{t}/2)$. Assuming this ansatz, the leading-order, short-time behaviour of η is governed by the forced wave equation:

$$\frac{\partial^2 \tilde{\eta}_0}{\partial \hat{t}^2} - \frac{1}{\kappa^2}\nabla_\perp^2 \tilde{\eta}_0 = -k_z \dot{\gamma}\frac{M}{\kappa}\hat{v}_k \mathrm{e}^{-\mathrm{i}\hat{t}}. \tag{4.23}$$

An example response is reported in figure 17. A shear wave can be identified in the contours of $|\partial\eta/\partial y|$ seen in figure 17(*a*). The wave undergoes multiple reflections

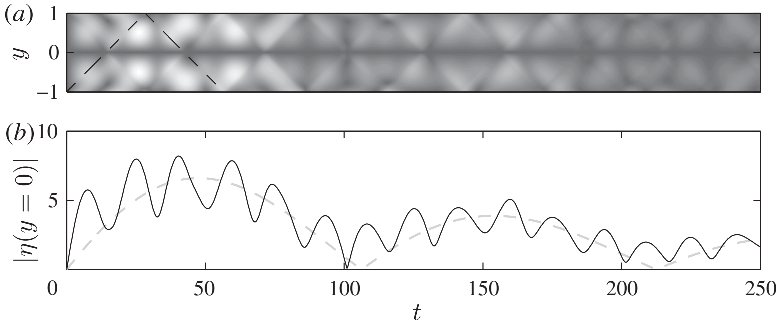

FIGURE 17. Solution in the instantaneously elastic limit ($\beta = 0$). Here $R = 2$, $W = 100$, which sets a wave speed $M^{-1} = 0.07$. (*a*) Contours of $|\partial\eta/\partial y|$, dashed black lines identify shear wave propagation. (*b*) Vertical vorticity at the centreline; the dashed grey line follows the envelope modulation at the beating frequency, plotted here as $|A_m \sin((\mathscr{K}_1 - \kappa)t/2M)\exp(-t/2W)|$.

from the walls. Interestingly, there are two clear frequencies in the vorticity amplitude (figure 17*b*): a short-time oscillation and a longer-scale modulation.

Extracting the two frequencies is easiest by constructing a solution to (4.23) with the method of images. Shifting the wall-normal coordinate $Y = y + 1$, and placing an infinite number of forcing images above and below the original domain, allows the solution to be expressed as a Fourier sine series, $\tilde{\eta}_0(Y, \hat{t}) = \sum_{n=1}^{\infty} \varphi_n(\hat{t})\sin(n\pi Y/2)$. Substituting this expansion into (4.23) and using the orthogonality property of the basis functions, the amplitudes are found from the system of ordinary differential equations:

$$\frac{\mathrm{d}^2\varphi_n}{\mathrm{d}\hat{t}^2} + \frac{\mathscr{K}_n^2}{\kappa^2}\varphi_n = -k_z\dot{\gamma}\frac{M}{\kappa}b_n\mathrm{e}^{-\mathrm{i}\hat{t}}, \tag{4.24}$$

where $\mathscr{K}_n^2 = k_z^2 + (n\pi/2)^2$, and the b_n are the Fourier coefficients of $\hat{v}_k$. The initial conditions are $\varphi_n(0) = 0$ and $\mathrm{d}_t\varphi_n(0) = -\mathrm{i}k_z\dot{\gamma}b_n - \mathrm{i}k_z\dot{\gamma}c_n$. The c_n are the coefficients of $\hat{v}_\lambda$. The Fourier amplitudes are therefore:

$$\varphi_n(\hat{t}) = D_n^+\exp(\mathrm{i}\mathscr{K}_n\hat{t}/\kappa) + D_n^-\exp(-\mathrm{i}\mathscr{K}_n\hat{t}/\kappa) + f_n\mathrm{e}^{-\mathrm{i}\hat{t}}, \tag{4.25}$$

with

$$D_n^{\pm} = \mp\left[\frac{k_z\dot{\gamma}M}{2(\mathscr{K}_n \pm \kappa)}b_n + \frac{k_z\dot{\gamma}M}{2\mathscr{K}_n}c_n\right], \quad f_n = -\frac{k_z\dot{\gamma}M\kappa}{\mathscr{K}_n^2 - \kappa^2}b_n. \tag{4.26}$$

The terms involving $D_n^{\pm}$ constitute the trapped vorticity waves, and the f_n term corresponds to the component of the response propagating in the span with the forcing. Furthermore, the solution demonstrates that the streak amplitude is set by the viscoelastic Mach number, M, consistent with the scaling in figure 16, where β is finite but small. With the first ten modes of the Fourier expansion, $n \sim 10$, the shear waves can be accurately resolved. However, the fast and slow frequencies are already contained in the evolution equation for the first Fourier mode. Rearranging the expression for the $\varphi_1(\hat{t})$, the two frequencies are found as:

$$\Omega_{fast} = \frac{\mathscr{K}_1 + \kappa}{2M}, \quad \Omega_{slow} = \frac{\mathscr{K}_1 - \kappa}{2M}. \tag{4.27}$$

The modulation is a manifestation of 'beating', which results from the slight disparity between the phase speed of the forcing, $c_z \approx \kappa/Mk_z$, and the phase speed of the trapped normal-vorticity waves, $c_\eta \approx \mathscr{K}_1/Mk_z$. The predicted beating frequency has been overlaid on figure 17(*b*).

We now briefly comment on the flow response to a stationary, pulsating streamwise vortex, which can be constructed from an equal superposition of O–S modes with $\omega = \omega^+$ and $\omega = \omega^-$. In this case there is no broken symmetry in the z–t plane, since Squire modes travelling in both $\pm z$ are excited equally. In special cases, the form of the forcing term to the Squire equation, $\mathscr{F}(y, t)$, triggers a standing wave only in the response. For example, for very low β, a roll of the form:

$$v'(y, z, t) = \hat{v}(y)\exp(\mathrm{i}k_z z - \mathrm{i}\omega^+ t) + \hat{v}(y)\exp(\mathrm{i}k_z z - \mathrm{i}\omega^- t) = 2\hat{v}(y)\cos(\omega_r t)\exp(\mathrm{i}k_z z)\exp(\omega_i t), \tag{4.28}$$

produces a Squire response which is a standing wave in the cross-flow plane, oscillating at the forcing frequency. In this instance, the initial conditions on the forcing term, $\mathscr{F}(y, t)$, and on $\partial_t \eta$ allow the response to immediately follow the forcing. For other forcing parameters, or rolls, this is not the case, and the response includes propagating and reflecting vertical-vorticity waves alongside this oscillatory component.

The low-Reynolds-number/high-elasticity behaviour identified in this section is distinct from the prediction by Jovanovic & Kumar (2010, 2011), which has been recovered in the current formulation in the limit $\Theta \gg 1$. The particular limit presented here for $\Theta \sim 1$, with very low β, may have relevance to polymer melts or very dense micellar solutions (Zhou *et al.* 2012). Importantly, the behaviour is retained in dilute solutions (i.e. as shown in figures 13–16), although vorticity waves cannot be identified due to the smoothing action of solvent diffusivity. The bounds on the region of finite frequency in the dispersion relation (3.18) provide some guidance as to the extent of the region where $\Theta \sim 1$ for a given polymer concentration, and hence when propagating vorticity waves (and streak re-energization) can be anticipated.

5. Conclusion

The mechanics of energy amplification in viscoelastic Couette flow were examined by considering the linear flow response to forcing from a decaying streamwise vortex. A key parameter which determines the nature of the forcing and the transient streak response is $\Theta = W\beta\kappa^2/R$, the ratio of the relaxation time to the disturbance diffusion time scale in the solvent.

The forcing vortex is an eigenfunction of the homogeneous Orr–Sommerfeld damped wave equation. It can have one of two complex frequencies, which were associated with a 'quasi-Newtonian' and an 'elastic' mode. (i) Forcing from the quasi-Newtonian mode produced streaks which collapse onto the Newtonian curves at the same total and solvent Reynolds numbers, when $\Theta \ll 1$ and $\Theta \gg 1$, respectively. When $\Theta \ll 1$ the polymer is instantly responsive on the solvent time scale, and produces a stress proportional to the rate of strain. In the opposite limit, $\Theta \gg 1$, the polymer is essentially frozen and the dynamics in the solvent decouple. (ii) Forcing from the elastic mode results in streaks growing and decaying like $t\exp(-t/W\beta)$ when $\Theta \gg 1$. The associated mechanism, polymer stretch, remains at low Reynolds numbers, and causes significant streak amplification even in inertialess flows.

When $\Theta \sim 1$, the decay rates of the quasi-Newtonian and the elastic modes coalesce. This wall-normal vorticity response in this regime is characterized by streak re-energization, a behaviour which becomes more prominent with decreasing solvent viscosity. Examination of the operator as $\beta \to 0$ revealed that the streak re-energization is a superposition of trapped vertical-vorticity waves.

The analysis highlights the wealth of possible dynamics that result from introducing polymer additives to a seemingly simple flow configuration. Although the wavenumber of the streamwise vortex, κ, was fixed in this study, its appearance in the parameter Θ is intriguing. It suggests that, in more complicated situations, the dominant dynamics will depend not only on the flow parameters, but also on the spectrum of perturbations present. An important question is whether the streamwise vortex would be observed in practice in a real flow. Previous linear analyses of the flow response to body forces in both Newtonian (Bamieh & Dahleh 2001; Jovanović & Bamieh 2005) and weak-inertia viscoelastic (Lieu *et al.* 2013) flows highlight a flow sensitivity to streamwise elongated disturbances with $O(1)$ spanwise spacing. This sensitivity underscores the importance of the current results.

The present work identified a rich variety of streak dynamics in viscoelastic Couette flow, despite adopting a very simple model for the polymeric liquid. Further work is required to assess how the growth mechanisms which were identified here are altered in more realistic polymer models that include, for example, the effects of shear thinning or finite polymer extensibility.

Appendix. Details of the initial value problems

Details of the Laplace-transform solutions to initial value problems discussed in the text are presented here.

A.1. *The general solution to the initial value problem*

The wall-normal vorticity response to forcing from the decaying streamwise vortex is governed by the initial boundary value problem:

$$\frac{\partial^2 \eta}{\partial t^2} + \left(\frac{1}{W} - \frac{\beta}{R}\nabla_\perp^2\right)\frac{\partial \eta}{\partial t} - \frac{1}{RW}\nabla_\perp^2 \eta = -\mathrm{i}k_z\dot{\gamma}\left[\left(\frac{1}{W} - \mathrm{i}\omega\right) - \frac{(1-\beta)}{R(1-\mathrm{i}\omega W)}\nabla_\perp^2\right]\hat{v}\mathrm{e}^{-\mathrm{i}\omega t}. \tag{A 1}$$

We solve for the temporal behaviour by taking a Laplace transform:

$$\eta^s(y, s) = \int_0^\infty \eta(y, t)\mathrm{e}^{-st}\,\mathrm{d}t. \tag{A 2}$$

Since all variables in the forced system are initially zero, the vertical vorticity inherits the initial condition on the polymer body force, $T_\eta(y, 0) = 0$, through the condition

$$\left.\frac{\partial \eta}{\partial t}\right|_{t=0} = -\mathrm{i}k_z\dot{\gamma}\,\hat{v}. \tag{A 3}$$

The Laplace transform leaves a two-point boundary value problem:

$$\frac{\mathrm{d}^2\eta^s}{\mathrm{d}y^2} - \left(k_z^2 + sR\frac{(1+sW)}{(1+sW\beta)}\right)\eta^s = \frac{\mathrm{i}k_z\dot{\gamma}R}{(s+\mathrm{i}\omega)(1+sW\beta)}\left((1+sW) - \frac{W(1-\beta)}{R(1-\mathrm{i}\omega W)}\nabla_\perp^2\right)\hat{v}. \tag{A 4}$$

The forcing is due to a symmetric eigenfunction, from which the general solution is found to be ($s \neq 0, -1/W, -\mathrm{i}\omega$):

$$\begin{aligned}\eta^s(y,s) \;=\; & \frac{\mathrm{i}k_z\dot{\gamma}A_k}{s(s+\mathrm{i}\omega)}\left(\frac{\cosh k_z}{\cosh\chi}\cosh(\chi y)-\cosh(k_z y)\right)\\ & + \frac{\mathrm{i}k_z\dot{\gamma}A_\lambda}{W(s+\mathrm{i}\omega)^2(s+\vartheta)}\left((1+sW)+\frac{\mathrm{i}\omega W(1-\beta)}{(1-\mathrm{i}\omega W\beta)}\right)\\ & \times\left(\frac{\cosh\lambda}{\cosh\chi}\cosh(\chi y)-\cosh(\lambda y)\right),\end{aligned} \qquad (\mathrm{A}\,5)$$

where

$$\chi(s)=\left(k_z^2+sR\frac{(1+sW)}{(1+sW\beta)}\right)^{1/2}, \quad \vartheta=\frac{(1-\mathrm{i}\omega W)}{W(1-\mathrm{i}\omega W\beta)}. \qquad (\mathrm{A}\,6)$$

The solution is invalid at the three points indicated above, since $\chi(s)=k_z$ in the case of $s=0, -1/W$ and $\chi(s)=\lambda$ if $s=-\mathrm{i}\omega$. The wall-normal vorticity operator is then forced by one of its homogeneous solutions, leading to resonant behaviour. The solutions when $\chi(s)=k_z$ are analytic at the points in the s-plane where they are valid and do not contribute to the inversion. The solution at $s=-\mathrm{i}\omega$ gives the particular response to the forcing mode in the frequency domain,

$$\begin{aligned}\eta^s(y,s) \;=\; & \frac{\mathrm{i}k_z\dot{\gamma}A_k}{s(s+\mathrm{i}\omega)}\left(\frac{\cosh k_z}{\cosh\chi}\cosh(\chi y)-\cosh(k_z y)\right)\\ & + \frac{\mathrm{i}k_z\dot{\gamma}RA_\lambda}{2\lambda(s+\mathrm{i}\omega)(1+sW\beta)}\left((1+sW)+\frac{\mathrm{i}\omega W(1-\beta)}{(1-\mathrm{i}\omega W\beta)}\right)\\ & \times\left(y\sinh(\chi y)-\frac{\sinh\lambda}{\cosh\chi}\cosh(\chi y)\right).\end{aligned} \qquad (\mathrm{A}\,7)$$

We can now invert back into the time domain with the Bromwich integral:

$$\eta(y,t)=\frac{1}{2\pi\mathrm{i}}\int_{\gamma-\mathrm{i}\infty}^{\gamma+\mathrm{i}\infty}\eta^s(y,s)\mathrm{e}^{st}\mathrm{d}s=\frac{1}{2\pi\mathrm{i}}\oint_C\eta^s(y,s)\mathrm{e}^{st}\mathrm{d}s, \qquad (\mathrm{A}\,8)$$

where γ is to the right of all singularities in the s-plane. The contour is closed with a semicircle to the left of γ. Since $\eta^s(y,s)$ has no branch points, the solution is the sum of the residues:

$$\eta(y,t)=\sum_j \mathrm{Res}\left[\eta^s(y,s)\mathrm{e}^{st}, s_j\right]. \qquad (\mathrm{A}\,9)$$

There are simple poles at $s=-\mathrm{i}\omega$ and the zeros of $\cosh\chi$, or equivalently $\chi^2=-(2j-1)^2\pi^2/4$, with $j=1,2,\ldots$. Upon expansion of χ the zeros of $\cosh\chi$ are seen to correspond to the symmetric eigenvalues of the homogeneous wall-normal vorticity equation, $s=-\mathrm{i}\omega^{\pm}_{\eta,j}$, with

$$\omega^{\pm}_{\eta,j}=-\frac{\mathrm{i}}{2W}\left(\frac{W\beta\kappa^2_{\eta,j}}{R}+1\pm\Phi_{\eta,j}\right), \qquad (\mathrm{A}\,10)$$

where $\kappa_{\eta,j}^2 = k_z^2 - \lambda_{\eta,j}^2$, with $\lambda_{\eta,j} = (2j-1)\mathrm{i}\pi/2$ the wall-normal wavenumbers, and

$$\Phi_{\eta,j}(\kappa_{\eta,j}; R, W, \beta) = \left[\left(1 + \frac{W\beta\kappa_{\eta,j}^2}{R}\right)^2 - \frac{4W\kappa_{\eta,j}^2}{R}\right]^{1/2}. \tag{A 11}$$

The homogeneous wall-normal vorticity eigenvalues satisfy a dispersion relation which has an identical form to that of the homogeneous subsystem, though there is an extra degree of freedom since the wall-normal vorticity gradient does not need to vanish at the wall. Summing the residues:

$$\begin{aligned}\eta(y,t) = {} & \left[\frac{\mathrm{i}k_z\dot{\gamma}RA_\lambda[1-\mathrm{i}\omega W\beta(2-\mathrm{i}\omega W)]}{2\lambda(1-\mathrm{i}\omega W\beta)^2}\Big(y\sinh(\lambda y) - \tanh\lambda\cosh(\lambda y)\Big) + \frac{k_z\dot{\gamma}}{\omega}\hat{v}\right]\mathrm{e}^{-\mathrm{i}\omega t} \\ & + \sum_{j=1}^{\infty}\frac{\mathrm{i}k_z\dot{\gamma}A_k\cosh k_z}{\phi_j\sinh\lambda_{\eta,j}}\left[\frac{1}{\omega_{\eta,j}^{\pm}(\omega-\omega_{\eta,j}^{\pm})} + \frac{1}{W(\omega-\omega_{\eta,j}^{\pm})^2(\vartheta - \mathrm{i}\omega_{\eta,j}^{\pm})}\right. \\ & \left.\times\left((1-\mathrm{i}\omega_{\eta,j}^{\pm}W) + \frac{\mathrm{i}\omega W(1-\beta)}{(1-\mathrm{i}\omega W\beta)}\right)\right]\cosh\left(\lambda_{\eta,j}y\right)\mathrm{e}^{-\mathrm{i}\omega_{\eta,j}^{\pm}t},\end{aligned} \tag{A 12}$$

with $\phi_j = \mathrm{d}_s\chi(-\mathrm{i}\omega_{\eta,j}^{\pm})$. The summation is carried out twice, once over each eigenvalue pair $\omega_{\eta,j}^{\pm}$. The solution consists of the forced vorticity eigenmode, complemented by a packet of homogeneous, even vorticity modes ($\hat{\eta}_h(y; j) = \cosh(\lambda_{\eta,j}y)$).

In the main body of the text, the solution is written as

$$\begin{aligned}\eta(y,t) = {} & \hat{\eta}_p(y)\mathrm{e}^{-\mathrm{i}\omega t} + \sum_{j=1}^{\infty} C_j(\omega_{\eta,j}^{+}; \omega, R, W, \beta)\cosh(\lambda_{\eta,j}y)\exp(-\mathrm{i}\omega_{\eta,j}^{+}t) \\ & + \sum_{j=1}^{\infty} C_j(\omega_{\eta,j}^{-}; \omega, R, W, \beta)\cosh(\lambda_{\eta,j}y)\exp(-\mathrm{i}\omega_{\eta,j}^{-}t).\end{aligned} \tag{A 13}$$

The terms appearing here, namely η_p and C_j, can be identified in the exact solution (A 12).

A.2. *Elastic mode with $\Theta \gg 1$*

When forcing is due to the elastic mode with $\Theta \gg 1$, the leading-order vertical vorticity on the solvent time scale is found from

$$\frac{\partial\tilde{\eta}_0}{\partial\tilde{t}} - \frac{1}{\kappa^2}\nabla_\perp^2\tilde{\eta}_0 = -\mathrm{i}k_z\dot{\gamma}\frac{R}{\beta\kappa^2}\hat{v} + \mathrm{i}k_z\dot{\gamma}\frac{R}{\beta\kappa^2}\hat{v}_\lambda\tilde{t}. \tag{A 14}$$

We take a Laplace transform in time to obtain an ordinary differential equation in y:

$$\frac{\mathrm{d}^2\eta_0^s}{\mathrm{d}y^2} - \left(k_z^2 + \tilde{s}\kappa^2\right)\eta_0^s = \mathrm{i}k_z\dot{\gamma}\frac{R}{\beta}\frac{1}{\tilde{s}}\hat{v} - \mathrm{i}k_z\dot{\gamma}\frac{R}{\beta}\frac{1}{\tilde{s}^2}\hat{v}_\lambda, \tag{A 15}$$

where $\tilde{s}$ is the transform variable for the solvent time scale.

The general solution, valid everywhere except $\tilde{s} = 0, -1$, is

$$\begin{aligned}\eta_0^s(y,\tilde{s}) = {} & \frac{\mathrm{i}k_z\dot{\gamma}RA_k}{\beta\kappa^2\tilde{s}^2}\left(\frac{\cosh k_z}{\cosh\zeta}\cosh(\zeta y) - \cosh(k_z y)\right) \\ & - \frac{\mathrm{i}k_z\dot{\gamma}RA_\lambda(1-\tilde{s})}{\beta\kappa^2\tilde{s}^2(1+\tilde{s})}\left(\frac{\cosh\lambda}{\cosh\zeta}\cosh(\zeta y) - \cosh(\lambda y)\right),\end{aligned} \tag{A 16}$$

with $\zeta(s)=\sqrt{k_z^2+\tilde{s}\kappa^2}$. At $\tilde{s}=0$ and $\tilde{s}=-1$, the operator is forced by one of its homogeneous solutions. The solution at $\tilde{s}=-1$ is analytic, so only the correction at $\tilde{s}=0$ is required:

$$\eta_0^s(y,\tilde{s}) = -\frac{\mathrm{i}\dot{\gamma}RA_k}{2\beta\tilde{s}}\Big(y\sinh(\zeta y)-\tanh k_z\cosh(\zeta y)\Big) - \frac{\mathrm{i}k_z\dot{\gamma}RA_\lambda(1-\tilde{s})}{\beta\kappa^2\tilde{s}^2(1+\tilde{s})}\left(\frac{\cosh\lambda}{\cosh\zeta}\cosh(\zeta y)-\cosh(\lambda y)\right). \tag{A 17}$$

There are simple and second-order poles at $\tilde{s}=0$, and simple poles at the zeros of $\cosh\zeta$ which are the rapidly decaying solvent vorticity modes. The lack of branch points means that the solution in physical space is obtained by summing the residues of $\eta_0^s(y,\tilde{s})\exp(\tilde{s}\tilde{t})$. In terms of the convective time scale the solution is written as:

$$\tilde{\eta}_0(y,t) = \mathrm{i}k_z\dot{\gamma}\,\hat{v}\,t-\frac{2\mathrm{i}k_z\dot{\gamma}R}{\beta\kappa^2}\hat{v}+\frac{\mathrm{i}\dot{\gamma}RA_k}{\beta}\Big(y\sinh(k_zy)-\tanh k_z\cosh(k_zy)\Big) + \sum_{j=1}^{\infty}\frac{2\mathrm{i}k_z\dot{\gamma}\beta A_\lambda\cosh\lambda}{\omega_{\eta,j}^2R(1-\mathrm{i}\omega_{\eta,j}R/\beta\kappa^2)}\frac{\lambda_{\eta,j}\cosh(\lambda_{\eta,j}y)}{\sinh\lambda_{\eta,j}}\exp(-\mathrm{i}\omega_{\eta,j}t), \tag{A 18}$$

where $\omega_{\eta,j}=-\mathrm{i}\beta\kappa_{\eta,j}^2/R$ are the rapidly decaying solvent Squire modes. Matching this solution to the inner limit of the outer solution (4.16), we find the function $N_0(y)$:

$$N_0(y)=-\frac{2\mathrm{i}k_z\dot{\gamma}R}{\beta\kappa^2}\hat{v}+\frac{\mathrm{i}\dot{\gamma}RA_k}{\beta}\Big(y\sinh(k_zy)-\tanh k_z\cosh(k_zy)\Big). \tag{A 19}$$

The uniformly valid composite solution is then found by combining the outer (4.16) and inner (A 18) solutions and subtracting their overlapping value:

$$\eta_0(y,t)=\mathrm{i}k_z\dot{\gamma}\,\hat{v}(y)t\mathrm{e}^{-t/W\beta}+N_0(y)\mathrm{e}^{-t/W\beta}+\sum_{j=1}^{\infty}S_j(\omega_{\eta,j};R,\beta)\cosh(\lambda_{\eta,j}y)\exp(-\mathrm{i}\omega_{\eta,j}t), \tag{A 20}$$

where S_j can be identified above in (A 18).

REFERENCES

ANDERSSON, P., BERGGREN, M. & HENNINGSON, D. S. 1999 Optimal disturbances and bypass transition in boundary layers. *Phys. Fluids* **11**, 134–150.

AZAIEZ, J. & HOMSY, G. M. 1994 Linear stability of free shear flow of viscoelastic liquids. *J. Fluid Mech.* **268**, 37–69.

BAMIEH, B. & DAHLEH, M. 2001 Energy amplification in channel flows with stochastic excitation. *Phys. Fluids* **13**, 3258.

BIRD, R. B., ARMSTRONG, R. C. & HASSAGER, O. 1987 *Dynamics of Polymeric Liquids,* vol.1. 2nd edn. Wiley.

BUTLER, K. M. & FARRELL, B. F. 1992 Optimal perturbations in viscous shear flow. *Phys. Fluids* A **4**, 1637–1650.

DENN, M. & PORTEOUS, K. 1971 Elastic effects in flow of viscoelastic liquids. *Chem. Engng J.* **2**, 280–286.

DOERING, C. R., ECKHARDT, B. & SCHUMACHER, J. 2006 Failure of energy stability in Oldroyd-B fluids at arbitrarily low Reynolds numbers. *J. Non-Newtonian Fluid Mech.* **135**, 92–96.

DUBIEF, Y., TERRAPON, V. E. & SORIA, J. 2013 On the mechanism of elasto-inertial turbulence. *Phys. Fluids* **25**, 110817.

DUBIEF, Y., WHITE, C. M., TERRAPON, V. E., SHAQFEH, E. S. G., MOIN, P. & LELE, S. K. 2004 On the coherent drag-reducing and turbulence-enhancing behaviour of polymers in wall flows. *J. Fluid Mech.* **514**, 271–280.

GRAHAM, M. D. 1999 The sharkskin instability of polymer melt flows. *Chaos* **9**, 154–163.

GROISMAN, A. & STEINBERG, V. 2000 Elastic turbulence in a polymer solution flow. *Nature* **405**, 53–55.

HODA, N., JOVANOVIĆ, M. R. & KUMAR, S. 2008 Energy amplification in channel flows of viscoelastic fluids. *J. Fluid Mech.* **601**, 407–424.

HODA, N., JOVANOVIĆ, M. R. & KUMAR, S. 2009 Frequency responses of streamwise-constant perturbations in channel flows of Oldroyd-B fluids. *J. Fluid Mech.* **625**, 411–434.

JAMES, D. F. 2009 Boger fluids. *Annu. Rev. Fluid Mech.* **41**, 129–142.

JOSEPH, D. D. 1990 *Fluid Dynamics of Viscoelastic Liquids*. Springer.

JOSEPH, D. D., NARAIN, A. & RICCIUS, O. 1986 Shear-wave speeds and elastic moduli for different liquids. Part 1. Theory. *J. Fluid Mech.* **171**, 289–308.

JOVANOVIĆ, M. R. & BAMIEH, B. 2005 Componentwise energy amplification in channel flows. *J. Fluid Mech.* **534**, 145–183.

JOVANOVIC, M. R. & KUMAR, S. 2010 Transient growth without inertia. *Phys. Fluids* **22**, 023101.

JOVANOVIC, M. R. & KUMAR, S. 2011 Nonmodal amplification of stochastic disturbances in strongly elastic channel flows. *J. Non-Newtonian Fluid Mech.* **166**, 755–778.

KUPFERMAN, R. 2005 On the linear stability of plane Couette flow for an Oldroyd-B fluid and its numerical approximation. *J. Non-Newtonian Fluid Mech.* **127**, 169–190.

LANDAHL, M. T. 1980 A note on an algebraic instability of inviscid parallel shear flows. *J. Fluid Mech.* **98**, 243–251.

LARSON, R. G. 2000 Turbulence without inertia. *Nature* **405**, 27–28.

LARSON, R. G., SHAQFEH, E. S. G. & MULLER, S. J. 1990 A purely elastic instability in Taylor–Couette flow. *J. Fluid Mech.* **218**, 573–600.

LIEU, B. K., JOVANOVIĆ, M. R. & KUMAR, S. 2013 Worst-case amplification of disturbances in inertialess Couette flow of viscoelastic fluids. *J. Fluid Mech.* **723**, 232–263.

MIN, T., YUL YOO, J., CHOI, H. & JOSEPH, D. 2003 Drag reduction by polymer additives in a turbulent channel flow. *J. Fluid Mech.* **486**, 213–238.

MOROZOV, A. N. & SAARLOOS, W. V. 2007 An introductory essay on subcritical instabilities and the transition to turbulence in visco-elastic parallel shear flows. *Phys. Rep.* **447**, 112–143.

NOUAR, C., BOTTARO, A. & BRANCHER, J. P. 2007 Delaying transition to turbulence in channel flow: revisiting the stability of shear-thinning fluids. *J. Fluid Mech.* **592**, 177–194.

PAN, L., MOROZOV, A., WAGNER, C. & ARRATIA, P. E. 2013 Nonlinear elastic instability in channel flows at low Reynolds numbers. *Phys. Rev. Lett.* **110**, 174502.

PREZIOSI, L. & JOSEPH, D. D. 1987 Stokes' first problem for viscoelastic fluids. *J. Non-Newtonian Fluid Mech.* **25**, 239–259.

RALLISON, J. M. & HINCH, E. J. 1995 Instability of a high-speed submerged elastic jet. *J. Fluid Mech.* **288**, 311–324.

RAY, P. K. & ZAKI, T. A. 2014 Absolute instability in viscoelastic mixing layers. *Phys. Fluids* **26**, 014103.

REDDY, S. C. & HENNINGSON, D. S. 1993 Energy growth in viscous channel flows. *J. Fluid Mech.* **252**, 209–238.

RENARDY, M. 2009 Stress modes in linear stability of viscoelastic flows. *J. Non-Newtonian Fluid Mech.* **159**, 137–140.

SAMANTA, D. S., DUBIEF, Y., HOLZNER, H., SCHÄFER, C., MOROZOV, A. N., WAGNER, C. & HOF, B. 2013 Elasto-inertial turbulence. *Proc. Natl Acad. Sci. USA* **110**, 10557–10562.

SCHMID, P. J. 2007 Nonmodal Stability Theory. *Annu. Rev. Fluid Mech.* **39**, 129–162.

SCHMID, P. J. & HENNINGSON, D. S. 2001 *Stability and Transition in Shear Flows*. Springer.

SHAQFEH, E. S. G. 1996 Purely elastic instabilities in viscometric flows. *Annu. Rev. Fluid Mech.* **28**, 129–185.

TANNER, R. I. 1962 Note on the Rayleigh problem for a visco-elastic fluid. *Z. Angew. Math. Phys.* **13**, 573–580.

TERRAPON, V. E., DUBIEF, Y., MOIN, P., SHAQFEH, E. S. G. & LELE, S. K. 2004 Simulated polymer stretch in a turbulent flow using Brownian dynamics. *J. Fluid Mech.* **504**, 61–71.

VAUGHAN, N. J. & ZAKI, T. A. 2011 Stability of zero-pressure-gradient boundary layer distorted by unsteady Klebanoff streaks. *J. Fluid Mech.* **681**, 116–153.

ZAKI, T. A. & DURBIN, P. A. 2005 Mode interaction and the bypass route to transition. *J. Fluid Mech.* **531**, 85–111.

ZHANG, M., LASHGARI, I., ZAKI, T. A. & BRANDT, L. 2013 Linear stability analysis of channel flow of viscoelastic Oldroyd-B and FENE-P fluids. *J. Fluid Mech.* **737**, 249–279.

ZHOU, L., COOK, L. P. & MCKINLEY, G. H. 2012 Multiple shear-banding transitions for a model of wormlike micellar solutions. *SIAM J. Appl. Math.* **72**, 1192–1212.